AD-A118 894 AERONAUTICAL RESEARCH LABS MELBOURNE (AUSTRALIA) F/G 1/3
AN INTERFEROMETRIC INVESTIGATION OF THE NEAR DESIGN POINT FLOW --ETC(U)
JAN 82 N POLLOCK
UNCLASSIFIED ARL/AERO-NOTE-405 NL

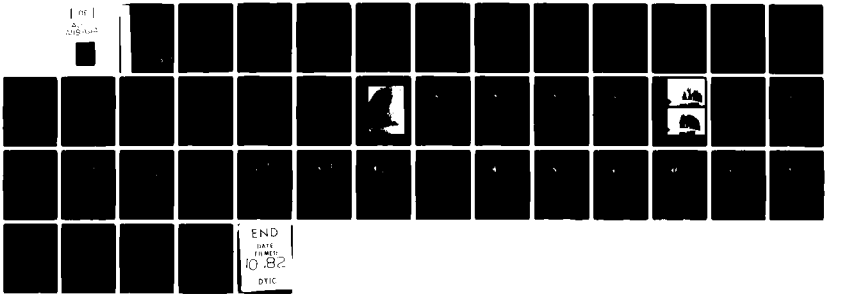

(12)

ARL/AERO-NOTE-405

AR-002-328

AUSTRALIA

DEPARTMENT OF DEFENCE

DEFENCE SCIENCE AND TECHNOLOGY ORGANISATION

AERONAUTICAL RESEARCH LABORATORIES

MELBOURNE, VICTORIA

AERODYNAMICS NOTE 405

AN INTERFEROMETRIC INVESTIGATION OF THE NEAR DESIGN POINT FLOW OVER SUPERCRITICAL AEROFOIL BGK-1

by

N. POLLOCK

Approved for Public Release

COPY No 3

JANUARY, 1982

AR-002-328

DEPARTMENT OF DEFENCE
DEFENCE SCIENCE AND TECHNOLOGY ORGANISATION
AERONAUTICAL RESEARCH LABORATORIES

AERODYNAMICS NOTE 405

AN INTERFEROMETRIC INVESTIGATION OF THE NEAR DESIGN POINT FLOW OVER SUPERCRITICAL AEROFOIL BGK-1

by

N. POLLOCK

SUMMARY

A recently developed laser interferometer was used to study the upper surface flow over supercritical aerofoil BGK-1 near its design condition. The tests were carried out at a chord Reynolds number of $1{\cdot}65 \times 10^6$ with transition free and artificially fixed at various chordwise locations. The interferograms were analysed to produce "instantaneous" surface pressure distributions for comparison with conventional time averaged distributions obtained from surface tappings.

The results show that the upper surface flow is unsteady with both fixed and free transition. They also indicate that artificially fixing transition in low Reynolds number tests does not produce an accurate simulation of the high Reynolds number flow for conditions near the design point.

POSTAL ADDRESS: Chief Superintendent, Aeronautical Research Laboratories,
Box 4331, P.O., Melbourne, Victoria, 3001, Australia.

CONTENTS

NOTATION

c	Model chord length
H	Total pressure of tunnel flow
M	Mach number
P	Static pressure acting on model
x	Streamwise ordinate measured from leading edge
y	Thickness ordinate measured from chord line
α	Model angle of incidence

1. INTRODUCTION

During the last 15 years many supercritical aerofoil sections have been designed and a number of these sections are now being used on production aircraft. Perhaps the most widely tested[1–7] of these sections is the profile designated BGK-1 designed by the numerical complex hodograph method of Bauer, Garabedian and Korn[8]. Although not intended to be a practical wing Section BGK-1 was designed to closely resemble some of the early semi-empirical NASA supercritical sections[9]. This similarity to practical empirical designs and the existence of an accurately known inviscid design pressure distribution explains the popularity of BGK-1 as a standard test aerofoil for wind tunnels and computational methods.

Some of the wind tunnel tests carried out on BGK-1 at a Reynolds number of $1{\cdot}6 \times 10^6$ and without artificial transition fixing show a pressure distribution at the design point in strikingly good agreement with theoretical predictions[8]. Higher Reynolds number tests[1,2] and tests with artificial transition fixing[4,6] showed significantly inferior agreement with theory. The available surface pressure distributions and schlieren and shadowgraph optical flow visualisation photographs do not contain sufficient information to explain these differences.

During 1979 a new laser interferometer system[10] was installed in the ARL transonic wind tunnel. It was decided to use the new flow visualisation capability provided by this system to further elucidate the nature of the near design point flow around supercritical aerofoil BGK-1. It was considered that the availability of interferograms of the flow would significantly increase the value of BGK-1 as a standard test aerofoil for both experimental and theoretical methods.

The tests described in this note were carried out in the transonic wind tunnel during September 1980.

2. EXPERIMENTAL DETAILS

2.1 Model

The BGK-1 aerofoil (Fig. 1) model used for these tests has a chord of 203·2 mm and a span of 532 mm. The design coordinates used for manufacturing were obtained from Reference 1. In the range $0{\cdot}00 \leqslant x/c \leqslant 0{\cdot}95$ the coordinates used for manufacturing were identical to the design coordinates (Table 1–1 and 1–2). For $x/c > 0{\cdot}95$ the coordinates were modified to produce a trailing edge thickness of $0{\cdot}0005c$ (Table 1–3). The measured profile errors for the completed model are plotted in Figure 2. On the more critical upper surface the accuracy achieved falls within the tolerances suggested in Reference 10 for this type of model (local waviness $< 0{\cdot}0002c$ and overall errors $< 0{\cdot}0005c$).

The model was made from a number of pieces of steel joined rigidly prior to the final machining of the profile. This enabled the surface pressure hole connections to be made without spoiling the windswept surfaces. The model had 37 pressure holes 0·4 mm diameter in the upper surface (Table 2). The holes were distributed over a span wise region 0 19c wide centred at midspan. The model was also equipped with pressure holes in the lower surface but they were not used in these tests.

For the tests conducted with fixed transition spanwise roughness bands comprising carborundum particles attached with lacquer were used. The bands were $1{\cdot}5\%c$ wide with a roughness height of approximately 0·15 mm. The lacquer layer was 0·03 mm thick and the roughness coverage was 10% to 20%.

2.2 Tunnel

The test section used was 533 mm wide and 813 mm high (Fig. 3). Solid sidewalls and longitudinally slotted top and bottom walls (open area ratio of 16·5% at the model location) were fitted. Mach number was derived from measurements of the pressure in the plenum chamber

surrounding the test section and the contraction entry, assuming these to be the static and total pressures of the test section flow respectively.

The model was supported by means of integral end tongues fitting into slots in sidewall mounted optical glass windows. The pressure lines were brought through the tongues to the outside of the test section.

There were gaps of 0·5 mm between the ends of the aerofoil section and the glass windows. Brief tests with these gaps sealed indicated that their presence did not affect the results.

2.3 Instrumentation

The model surface pressures were measured using two "Scanivalve" pressure multiplexers fitted with $\pm 33 \cdot 5$kPa differential pressure transducers referenced to tunnel static pressure. Stagger scanning was used to ensure the maximum settling time between readings. Scanning speed was 14 ports per second, with free stream conditions being recorded after each group of 12 ports. The model pressure tappings and connecting tube between model and scanivalve form a pneumatic low pass filter with a time constant of the order of 1 second. therefore pressure fluctuations at more than a few Hertz will not appear in the resulting pressure distributions.

The laser interferometer used is described in Reference 11. The field of view available with this instrument was slightly greater than half the area of the 406 mm diameter tunnel windows. The interferometer was therefore arranged so that the model upper surface was visible and the flow over the less interesting (for this type of aerofoil) lower surface was not recorded. The interferograms obtained were analysed to produce surface pressure distributions using the method described in the Appendix. The exposure time used in the interferometric investigation was 5 μsec. so pressure fluctuations at up to about 100 kHz should be reproduced. A typical interferogram is reproduced in Figure 4. Since the fringes are difficult to follow in some areas the interferometric data have been provided in the form of fringe tracings (Figs 5–8 and 10–25) rather than photographic reproductions.

The arrangement of the interferometer (Ref. 11) is such that the effect of vibration is to uniformly stretch or compress the fringe pattern in a direction normal to the aerofoil chord. Empty tunnel tests indicate that this effect is less than one fringe over the whole field. There is no mechanism for mechanical vibration to produce local variations in the fringe pattern. Previous tests with the interferometer have confirmed that accurate, reproducible interferograms are obtained when the flow is known to be steady.

When comparing surface pressure measurements with pressure distributions reduced from interferograms it should be remembered that the former are measured near midspan and the latter are a full span average (see Appendix). However at the low incidence angles of these tests the flow should be highly two-dimensional and the difference should not materially affect comparisons between the two measurements. There is a possibility that unsteadiness confined to the tunnel side wall boundary layers will be visible in the interferograms, but since the wall boundary layer thickness is small compared to the tunnel width this should not be a significant problem.

2.4 Test Program

Previous tests[8] on this aerofoil in the same wind tunnel have shown that the experimental design point (i.e. the test conditions which best reproduce the theoretical upper surface design pressure distribution) occurs at $M = 0 \cdot 783$ and $\alpha = 1 \cdot 7°$. The present test program was therefore centered on these values.

The difference between the experimental design conditions $M = 0 \cdot 783$, $\alpha = 1 \cdot 7°$ and the theoretical design values $M = 0 \cdot 75$, $\alpha = 0°$ is due partly to the effects of viscosity and partly due to tunnel interference. When corrected for tunnel interference[18] the experimental design conditions become $M = 0 \cdot 760$, $\alpha = 0 \cdot 50°$.

The chord Reynolds number for this series of tests was $1 \cdot 65 \pm 0 \cdot 05 \times 10^6$. Several interferograms were produced at some test conditions to provide information on flow steadiness. (The particular cases tested are listed in the table below:)

M	α	Transition	Figure Numbers
0·783	1·7°	Free	4–9
0·775	1·7°	Free	10
0·780	1·7°	Free	11
0·788	1·7°	Free	12
0·793	1·7°	Free	13
0·783	1·2°	Free	14
0·783	1·5°	Free	15
0·783	1·9°	Free	16
0·783	2·1°	Free	17
0·783	1·7°	Fixed at 2%c	18–20
0·783	1·7°	Fixed at 5%c	21
0·783	1·7°	Fixed at 17%c	22 and 23
0·783	1·7°	Fixed at 37%c	24 and 25

3. RESULTS AND DISCUSSION

3.1 Transition Free, Design Conditions

In Figures 5 to 8 four interferograms of the experimental design point flow ($M = 0{\cdot}783$, $\alpha = 1{\cdot}7°$) with transition free are presented. Pressure distributions reduced from the interferograms are also presented along with measured surface pressure distributions and the design pressure distribution. The four measured surface distributions are very nearly identical and in good agreement with the theoretical distribution. Previous work[8] has shown that M and α increments of 0·002 and 0·1° respectively, markedly reduced the agreement with the theoretical distribution.

Unlike the measured surface distributions the pressure distributions reduced from the interferograms showed considerable variations particularly near the end of the supersonic region at $0{\cdot}4 < x/c < 0{\cdot}7$. The interferograms (Fig. 4) and schlieren flow visualisation (Fig. 9) indicate that boundary layer transition takes place in this x/c range. The interferograms also show that away from the model surface the initial expansion near the leading edge (fringes sloping upwards to the right) is followed by a region of recompression (fringes sloping downwards to the right). This recompression terminates in the range $0{\cdot}4 < x/c < 0{\cdot}5$ and is followed by another expansion and compression. In some cases (e.g. Fig. 8) further weaker expansions and compressions occur prior to the final smooth subsonic recompression approaching the trailing edge. This cyclic expansion and compression is also evident in the long exposure schlieren photograph in Figure 9. Some of the interferograms (e.g. Fig. 7) show lines formed by the confluence of fringes indicating shock waves. Similar shock waves are evident in the short exposure schlieren photograph in Figure 9. Two of the reduced interferogram pressure distributions (Figs 5 and 8) show a pressure plateau typical of a shock induced laminar boundary layer separation followed by a turbulent reattachment[14]. The two others (Figs 6 and 7) do not show a clear plateau but the highly curved fringes in the interferograms near the model surface in the range $0{\cdot}5 < x/c < 0{\cdot}7$ indicates that the boundary layer displacement surface is significantly distorted.

The conclusion to be drawn from the above observations is that an unsteady laminar/transitional shock wave boundary layer interaction occurs in the range $0{\cdot}5 < x/c < 0{\cdot}7$. The test Reynolds number appears to be such that a significant laminar separation bubble is present for some of the time only. The significance of the fact that the time averaged pressure distribution (as measured by the surface tappings) is smooth and in good agreement with the theoretical distribution is not clear.

It is suggested that this design point flow may be useful as a particularly difficult test case for numerical Navier–Stokes equation solutions. The strong link between the boundary layer transition process and the outer flow would place particular emphasis on the correct representation of the physics of the flow in the numerical formulation.

3.2 Transition Free, Off Design Conditions

At Mach numbers below the design value and at the design incidence (Figs 10 and 11) both the measured surface pressures and the reduced interferograms show that the initial supersonic recompression is somewhat steeper than the design case with a significant reexpansion preceding the final recompression to subsonic speed. At Mach numbers above the design value (Figs 12 and 13) the initial supersonic recompression tends to develop into a pressure plateau with a final steep recompression to subsonic speed.

At incidence angles below the design value and at the design Mach number (Figs 14 and 15) the initial recompression is steeper than the design case with a pressure plateau or very weak expansion preceding the final return to subsonic speed. At incidence angles above the design value (Figs 16 and 17) the initial recompression is weakened with a rapid final return to subsonic speed involving shock waves.

The differences between the measured surface pressures and those reduced from the interferograms indicates that, as for the design point tests, the flow is quite unsteady under close to design conditions. Comparing the off-design (Figs 10–17) and design point (Figs 5–8) results it is evident that the time averaged design distribution evolves smoothly from the off-design distributions as the values of M and α are varied. As noted previously very small increments of M and α produce significant changes in the time averaged pressure distributions. The interferograms and the "instantaneous" pressure distributions derived from them show considerable variation and it would be difficult to distinguish between design and off-design conditions on this basis alone (see for example Figs 7 and 10). This again raises the question of the significance of the time averaged pressure distribution in an unsteady flow. It is tempting to consider the time averaged flow as the underlying steady flow on which are superimposed random fluctuations caused by tunnel flow unsteadiness. The alternative possibility is that the flow is inherently unstable and that the time averaged flow is not in itself a legitimate or possible flow. Numerical calculations would be valuable in resolving this question.

The off-design results (Figs 10 to 17) show that boundary layer transition (indicated by the appearance of the broken line showing the visible edge of the turbulent boundary layer) and the termination of the initial smooth supersonic recompression are closely associated. On the evidence available it is not possible to state which one causes the other, if indeed they do have a cause and effect relationship. Numerical calculations may also be useful in answering this question.

3.3 Transition Fixed

Results of tests with transition fixed at 2%c are presented in Figures 18–20. This transition location is in the subsonic part of the leading edge expansion and does not in itself produce a major impact on the pressure distribution or the interferogram. The resulting pressure distributions and interferograms have some similarity with the transition free results at less than the design Mach number (Fig. 10). However previous tests[4] have shown that the agreement between the transition fixed results and the theoretical design pressure distribution is not improved by varying the Mach number or incidence. The most probable mechanism for transition fixing to alter the design point pressure distribution is the alteration of the effective section displacement surface by the relatively thick turbulent boundary layer. This is consistent with the known sensitivity of this type of aerofoil to small changes in surface shape. Comparing Figures 18–20 it is evident that the flow has significant unsteadiness. This observation suggests that the unsteadiness noted in the transition free tests was not caused solely by the presence of an unsteady laminar boundary layer separation.

Moving the transition strip aft to 5% c (Fig. 21) does not appear to have any fundamental effect on the nature of the flow. Moving the transition strip further aft to 17% c where it is well into the supersonic region (Figs 22, 23) produces a large disturbance which extends well out into the flow. Despite this disturbance, which is clearly visible in the interferograms, the agreement between the surface pressure distributions and the design distribution is not significantly degraded over the forward transition cases discussed previously. This flow disturbance is believed to be due to the change in slope of the boundary layer displacement surface following transition rather than the obstruction produced by the transition strip itself. This view is supported by

the inviseid calculations of the effect of roughness bands presented in Reference 4. Moving the roughness band back to 37% c (Figs 24, 25) simply moves the flow disturbance aft. The results with transition at 17% c and 37% c (Figs 22–25) all show evidence of significant flow unsteadiness.

4. CONCLUSION

A recently developed laser interferometer has been used to study the upper surface flow over supercritical aerofoil BGK-1 near its design condition. The interferograms have been analysed to produce "instantaneous surface pressure distributions" which are compared with conventional time averaged pressure distributions obtained from surface tappings. These new data should considerably enhance the value of BGK-1 as a standard test aerofoil for experimental and theoretical methods.

The smooth "design" pressure distribution noted in previous transition free tests was found to be the time average of a very unsteady flow associated with unsteady boundary layer transition. It is not clear from the evidence available whether a laminar separation bubble is present some or all of the time at the design point. The significance of the excellent agreement between the theoretical design pressure distribution and the time average of a very unsteady flow appears to warrant further investigation.

Tests with boundary layer transition fixed with roughness bands indicated that transition locations in the supersonic region caused large distortions of the flow field for a significant distance from the model. Transition locations in the subsonic expansion near the nose did not obviously distort the flow, but the resulting thick turbulent boundary layer did destroy the agreement between theoretical and experimental design point pressure distributions. All the transition fixed tests showed evidence of flow unsteadiness which suggests that the transition free unsteadiness was not caused simply by unsteady transition location or laminar separation. It appears that, for this type of section, artificial transition fixing cannot be used to accurately simulate high Reynolds number conditions near the design point in low Reynolds number tunnel tests.

REFERENCES

1. J. J. Kacprzynski, L. H. Ohman, P. R. Garabedian and D. G. Korn—Analysis of the flow past a shockless lifting aerofoil in design and off-design conditions. NRC, NAE Report LR-554, 1971.
2. J. J. Kacprynski—An experimental analysis and buffet investigation of the shockless lifting aerofoil No. 1. NRC, NAE Report LR-569, 1973.
3. N. Pollock and B. D. Fairlie—An investigation of supercritical aerofoil BGK-1—Part 1: Near design point tests and comparisons with theory. ARL Report A/144, 1975.
4. N. Pollock and B. D. Fairlie—An investigation of supercritical aerofoil BGK-1—Part 2: Test Reynolds number requirements and transition fixing. ARL Report A/145, 1975.
5. B. D. Fairlie and N. Pollock—An investigation of supercritical aerofoil BGK-1—Part 3: Extended subsonic and transonic tests. ARL Report A/146, 1975.
6. B. F. L. Hammond—Results of tests on aerofoil M. 81/5 (BGK-1) in the ARA two dimensional tunnel. ARA Model Test Note M. 81/5, 1978.
7. M. A. Ramaswamy, K. Krishnamurthy and Ramachandra Sharma—Transonic wind tunnel tests on a supercritical aerofoil. NAL TM, AE-TM-24-74, 1974.
8. F. Bauer, P. R. Garabedian and D. G. Korn—Supercritical wing sections. (Lecture notes in economics and mathematical systems, Vol. 66.) Springer-Verlag, Berlin 1972.
9. R. T. Whitcomb—Review of NASA supercritical aerofoils. ICAS Paper 74-10, 1974.
10. R. C. Lock—A proposal for co-operative aerofoil tests in commonwealth transonic wind tunnels. CAARC CC 729, 1975.
11. N. Pollock—A simple laser interferometer for wind tunnel flow visualisation. Journal of physics E: Scientific instruments, Vol. 13, pp. 1062-66, 1980.
12. L. H. Tanner—The design and use of interferometers in aerodynamics. ARC R & M 3131, 1959.
13. B. D. Fairlie and N. Pollock—Evaluation of wall interference effects in a two-dimensional transonic wind tunnel by subsonic linear theory. ARL Report A/151, 1979.
14. J. Ackeret, F. Feldmann and N. Rott—Investigations of compression shocks and boundary layers in gases moving at high speed. NACA TM-1113, 1947.

TABLE 1-1

Profile of Aerofoil

Upper Surface—Design and Model

$0{\cdot}00 \leqslant x/c \leqslant 0{\cdot}95$

$\frac{x}{c}$	$\frac{y}{c}$	$\frac{x}{c}$	$\frac{y}{c}$	$\frac{x}{c}$	$\frac{y}{c}$
0·00000	0·00219	0·07532	0·04352	0·27237	0·06271
0·00001	0·00298	0·07597	0·04366	0·28741	0·06336
0·00006	0·00403	0·07660	0·04379	0·30299	0·06396
0·00017	0·00528	0·07724	0·04392	0·31906	0·06450
0·00027	0·00603	0·07786	0·04405	0·33556	0·06496
0·00039	0·00673	0·07849	0·04418	0·35232	0·06535
0·00058	0·00758	0·07911	0·04430	0·36959	0·06566
0·00080	0·00832	0·08045	0·04457	0·38700	0·06588
0·00109	0·00913	0·07978	0·04444	0·40413	0·06602
0·00141	0·00987	0·08253	0·04496	0·42139	0·06608
0·00154	0·01015	0·08113	0·04470	0·43871	0·06604
0·00215	0·01124	0·08182	0·04483	0·45601	0·06592
0·00269	0·01203	0·08327	0·04510	0·47325	0·06572
0·00333	0·01286	0·08404	0·04524	0·49034	0·06542
0·00428	0·01392	0·08484	0·04539	0·50724	0·06504
0·00534	0·01498	0·08574	0·04555	0·52388	0·06457
0·00689	0·01637	0·08670	0·04572	0·53954	0·06405
0·00865	0·01778	0·08773	0·04589	0·55487	0·06345
0·01107	0·01953	0·08885	0·04608	0·56982	0·06478
0·01458	0·02178	0·09006	0·04628	0·58435	0·06203
0·01964	0·02464	0·09138	0·04650	0·59841	0·06122
0·02348	0·02658	0·09282	0·04674	0·61194	0·06035
0·02831	0·02881	0·09441	0·04699	0·62490	0·05943
0·03389	0·03116	0·09626	0·04728	0·63727	0·05847
0·03779	0·03267	0·09831	0·04759	0·64844	0·05754
0·04089	0·03380	0·10058	0·04793	0·65902	0·05659
0·05268	0·03766	0·10310	0·04829	0·66899	0·05564
0·05397	0·03805	0·10591	0·04869	0·67832	0·05469
0·05543	0·03848	0·10901	0·04912	0·68701	0·05377
0·05692	0·03891	0·11245	0·04959	0·69509	0·05288
0·05769	0·03913	0·11625	0·05009	0·70694	0·05149
0·05846	0·03935	0·12062	0·05064	0·72841	0·04877
0·05922	0·03956	0·12545	0·05124	0·73865	0·04738
0·05997	0·03977	0·13078	0·05187	0·76139	0·04410
0·06071	0·03997	0·13664	0·05254	0·77701	0·04168
0·06145	0·04017	0·14305	0·05324	0·79224	0·03920
0·06217	0·04037	0·15004	0·05398	0·80907	0·03633
0·06291	0·04056	0·15763	0·05474	0·82499	0·03349
0·06444	0·04096	0·16585	0·05552	0·83695	0·03128
0·06593	0·04133	0·17493	0·05634	0·85719	0·02742
0·06738	0·04169	0·18470	0·05717	0·87562	0·02379
0·06879	0·04204	0·19518	0·05801	0·89827	0·01923
0·07016	0·04236	0·20636	0·05884	0·91369	0·01610
0·07148	0·04267	0·21825	0·05967	0·92769	0·01328
0·07277	0·04296	0·23081	0·06048	0·93981	0·01087
0·07401	0·04324	0·24405	0·06126		
0·07467	0·04338	0·25792	0·06201		

TABLE 1-2

Profile of Aerofoil

Lower Surface—Design and Model

$0{\cdot}00 \leqslant x/c \leqslant 0{\cdot}95$

$\frac{x}{c}$	$\frac{y}{c}$	$\frac{x}{c}$	$\frac{y}{c}$
0·00001	0·00149	0·26400	−0·05141
0·00004	0·00080	0·28205	−0·05150
0·00018	−0·00068	0·29705	−0·05144
0·00025	−0·00114	0·31015	−0·05128
0·00035	−0·00169	0·32408	−0·05103
0·00046	−0·00219	0·34487	−0·05046
0·00068	−0·00301	0·36350	−0·04976
0·00101	−0·00395	0·38765	−0·04860
0·00148	−0·00500	0·40449	−0·04763
0·00188	−0·00575	0·42631	−0·04616
0·00232	−0·00649	0·45002	−0·04432
0·00306	−0·00760	0·47538	−0·04206
0·00420	−0·00903	0·52184	−0·03720
0·00475	−0·00964	0·54984	−0·03383
0·00578	−0·01069	0·57861	−0·03008
0·00704	−0·01181	0·60531	−0·02636
0·00827	−0·01279	0·62348	−0·02373
0·00997	−0·01401	0·64215	−0·02096
0·01229	−0·01547	0·65754	−0·01865
0·01535	−0·01718	0·67121	−0·01659
0·01928	−0·01911	0·69034	−0·01373
0·02534	−0·02170	0·70889	−0·01101
0·02938	−0·02324	0·72669	−0·00850
0·03910	−0·02653	0·74668	−0·00585
0·05252	−0·03034	0·76850	−0·00322
0·06247	−0·03278	0·78489	−0·00148
0·07333	−0·03514	0·80115	0·00006
0·08529	−0·03744	0·81919	0·00149
0·09982	−0·03988	0·83855	0·00273
0·11856	−0·04253	0·85882	0·00369
0·14099	−0·04511	0·87943	0·00431
0·16719	−0·04745	0·90372	0·00459
0·20293	−0·04966	0·92651	0·00439
0·22851	−0·05068	0·94365	0·00395
0·24790	−0·05117		

TABLE 1-3

Profile of Aerofoil

$0{\cdot}95 \leqslant x/c \leqslant 1{\cdot}00$

Upper Surface

$\frac{x}{c}$	$\frac{y}{c}$ Design	$\frac{y}{c}$ Model
0·95200	0·00849	0·00851
0·97179	0·00480	0·00488
0·98910	0·00182	0·00200
0·99786	0·00048	0·00071
1·00000	0·00018	0·00043

Lower Surface

$\frac{x}{c}$	$\frac{y}{c}$ Design	$\frac{y}{c}$ Model
0·95867	0·00333	0·00327
0·97362	0·00247	0·00238
0·98619	0·00154	0·00138
0·99658	0·00056	0·00034
1·00000	0·00018	−0·00001

TABLE 2

Pressure Hole Locations

Upper Surface	
$\frac{x}{c}$	$\frac{y}{c}$
0·0000	0·0047
0·0035	0·0129
0·0079	0·0179
0·0196	0·0247
0·0294	0·0293
0·0495	0·0367
0·0741	0·0433
0·0991	0·0480
*0·1241	0·0513
0·1591	0·0549
0·1994	0·0583
0·2382	0·0609
0·2794	0·0631
0·3188	0·0645
0·3594	0·0655
0·3993	0·0660
0·4194	0·0660
0·4395	0·0660
0·4585	0·0659
0·4787	0·0656
0·4983	0·0653
0·5184	0·0648
0·5396	0·0641
0·5592	0·0632
0·5787	0·0624
0·5989	0·0612
0·6180	0·0599
0·6484	0·0576
0·6747	0·0551
0·6989	0·0525
0·7237	0·0494
0·7488	0·0459
0·7738	0·0422
0·7990	0·0381
0·8240	0·0339
0·8489	0·0289
0·8989	0·0191

* Damaged orifice.

APPENDIX

Interferogram Analysis

The basic expression for analysing interferograms of two dimensional isentropic flows[12] is:

$$\frac{P}{H} = \left[\left(\frac{Pr}{H}\right)^{1/\gamma} + \frac{\lambda R T_0}{KLH} \cdot N\right]^{\gamma}$$

where

P = Static pressure at any fringe

H = Tunnel stagnation pressure

Pr = Reference pressure (i.e. pressure at fringe "0")

T_0 = Tunnel stagnation temperature

L = Effective tunnel width (with allowance for tunnel sidewall boundary layers)

R = Gas constant

K = Gladstone Dale constant

λ = Wavelength of light used

γ = Ratio of specific heats

N = Fringe number where P is required.

For all the cases presented in this Note Fringe "0" was taken to be the first visible fringe to meet the model surface near the leading edge. The value of Pr for this fringe was obtained by interpolating the measured surface pressures.

The value of the parameter $\lambda R/KL$ was obtained by analysing the relatively steady monotonic compression which occurs over the forward 30% of chord. Comparing the number of fringes in this region with surface pressure distributions for five separate test cases produced a consistent value for $\lambda R/KL$. This procedure evaluates the otherwise unknown effective tunnel width.

The determination of the fringe number N is usually quite straightforward if the flowfield is worked through methodically starting with the reference fringe. However when shockwaves appear they tend to subdivide the flow into separate regions. Fortunately for all the cases presented here the shock waves were sufficiently short for an unbroken fringe to be found over the top of the shock effectively linking the two regions.

All the shock waves present in the tests reported here are considered to be sufficiently weak for the above isentropic analysis to give accurate results.

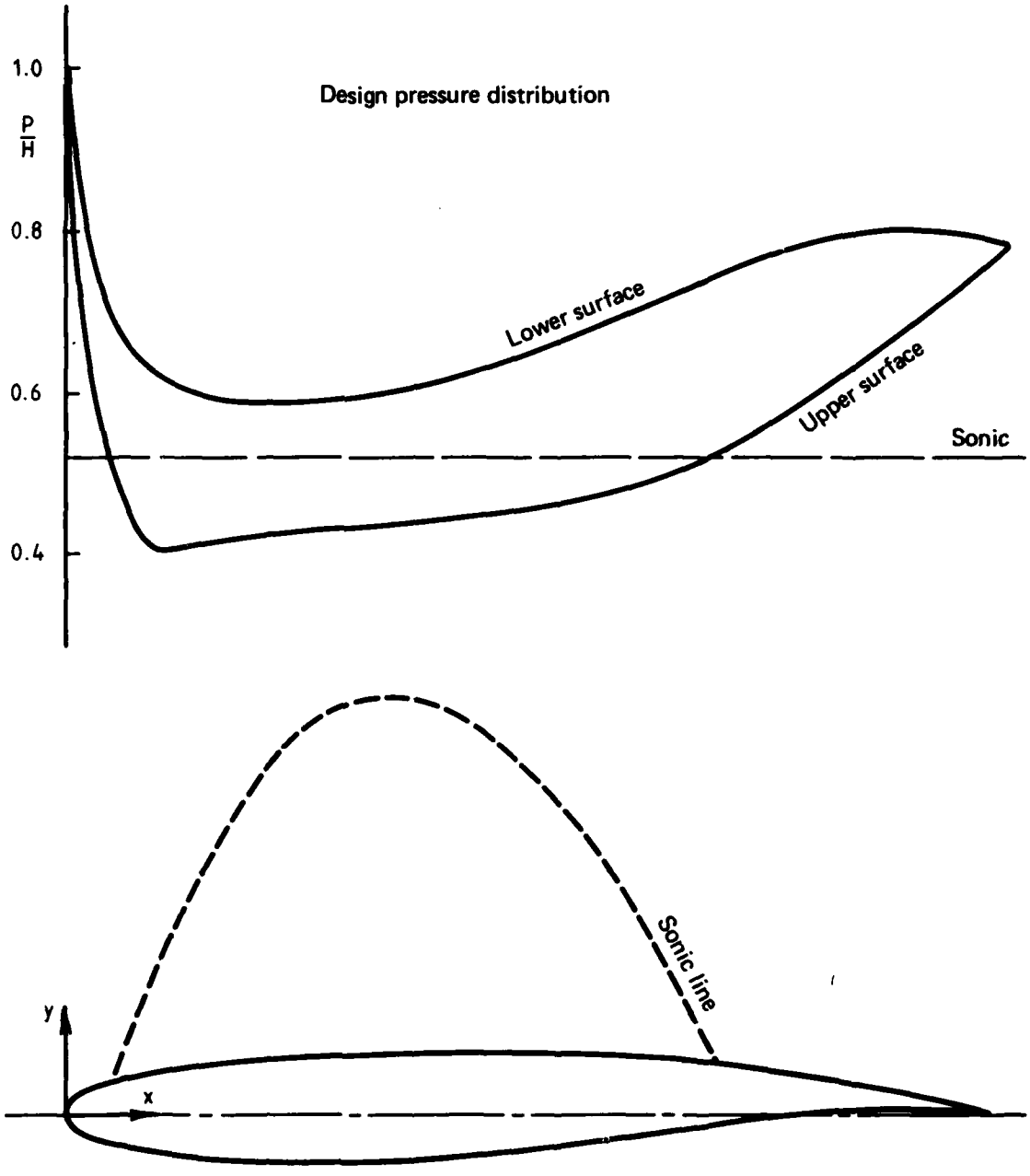

Thickness/Chord = 0,115

Design conditions M = 0,750 $\alpha = 0°$ $C_L = 0,63$

FIG. 1 SUPERCRITICAL LIFTING AEROFOIL BGK1

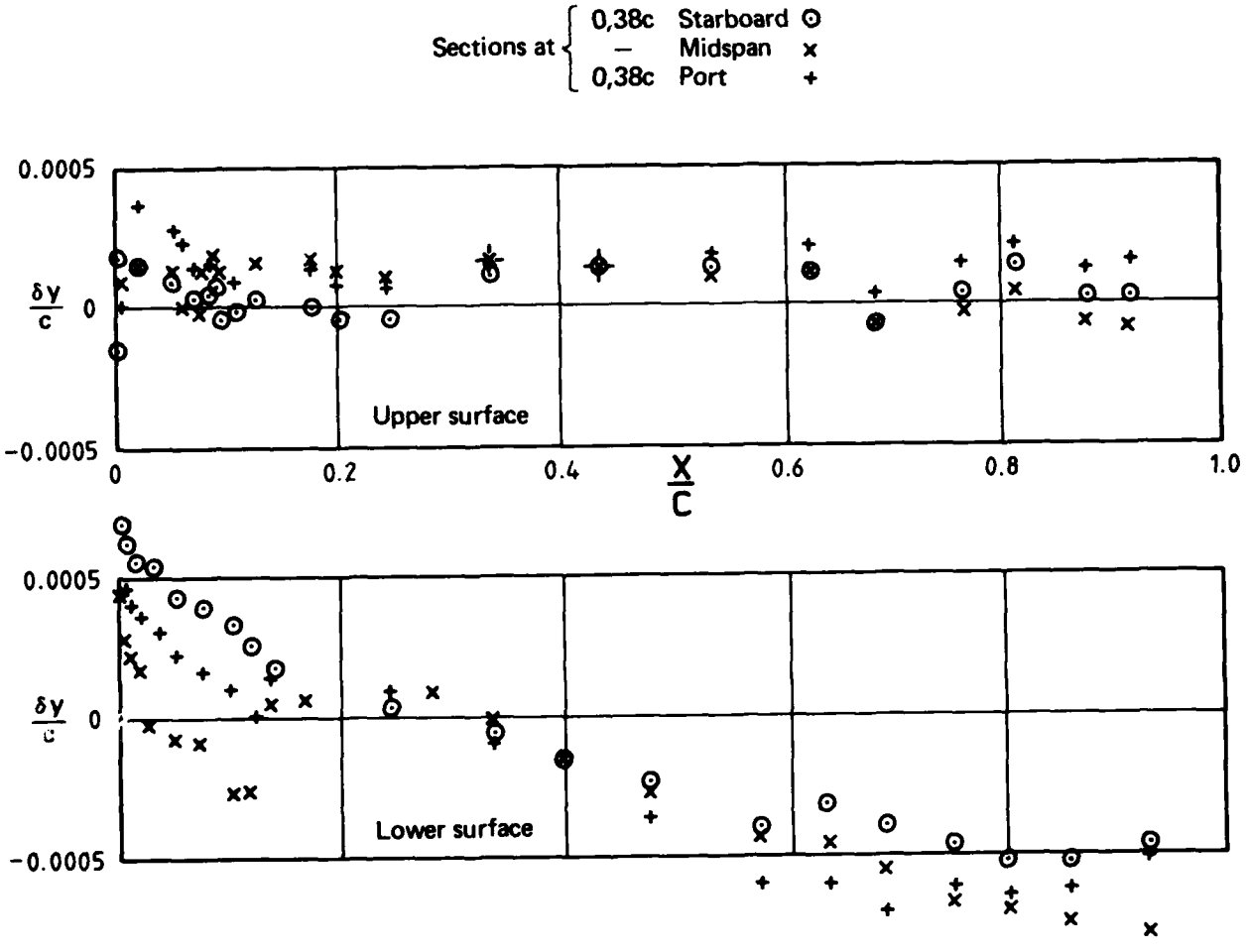

δy = Measured ordinate – Manufacturing ordinate
(positive for excess metal)

FIG. 2 PROFILE ERRORS

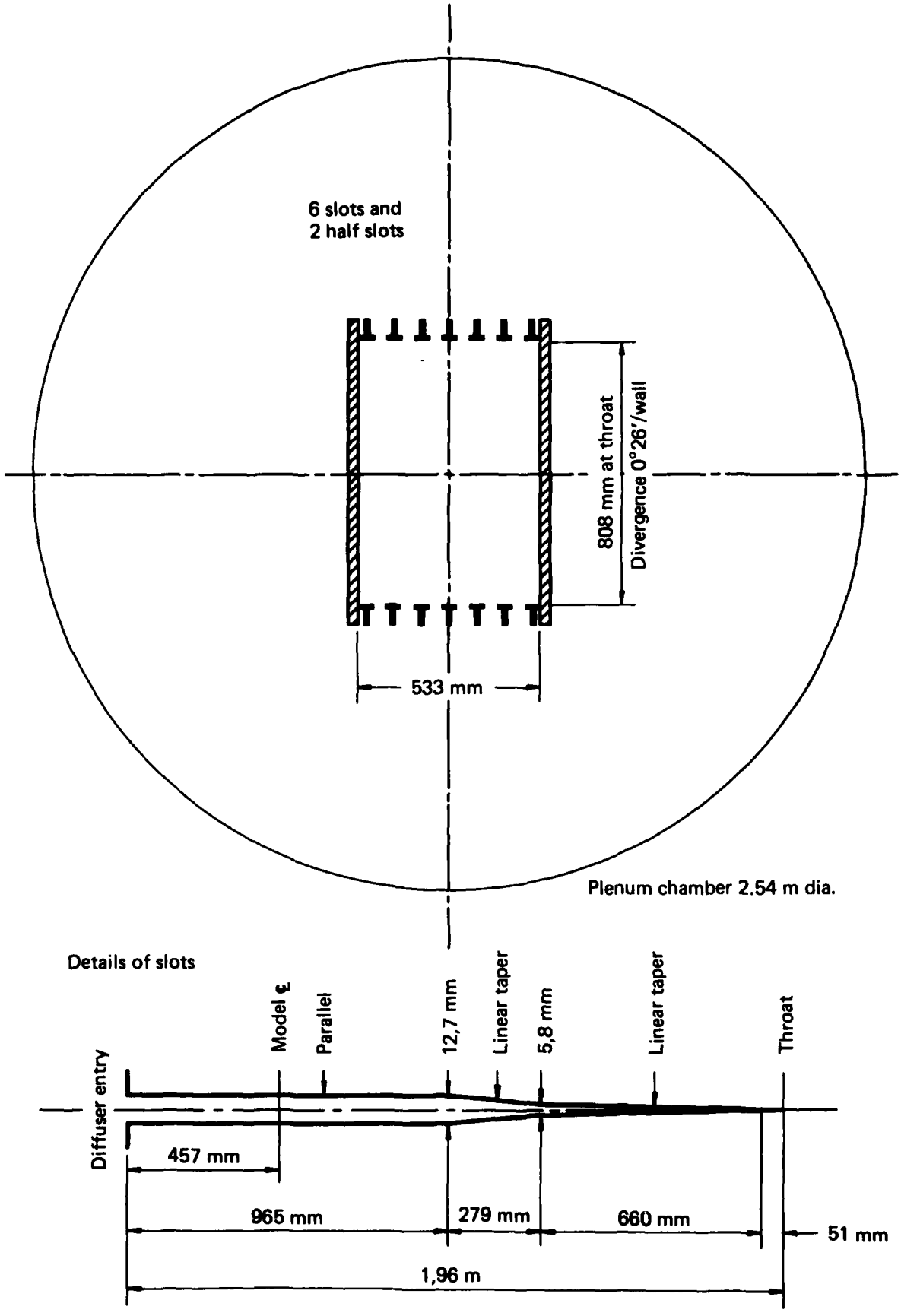

FIG. 3 DETAILS OF SLOTTED WORKING SECTION

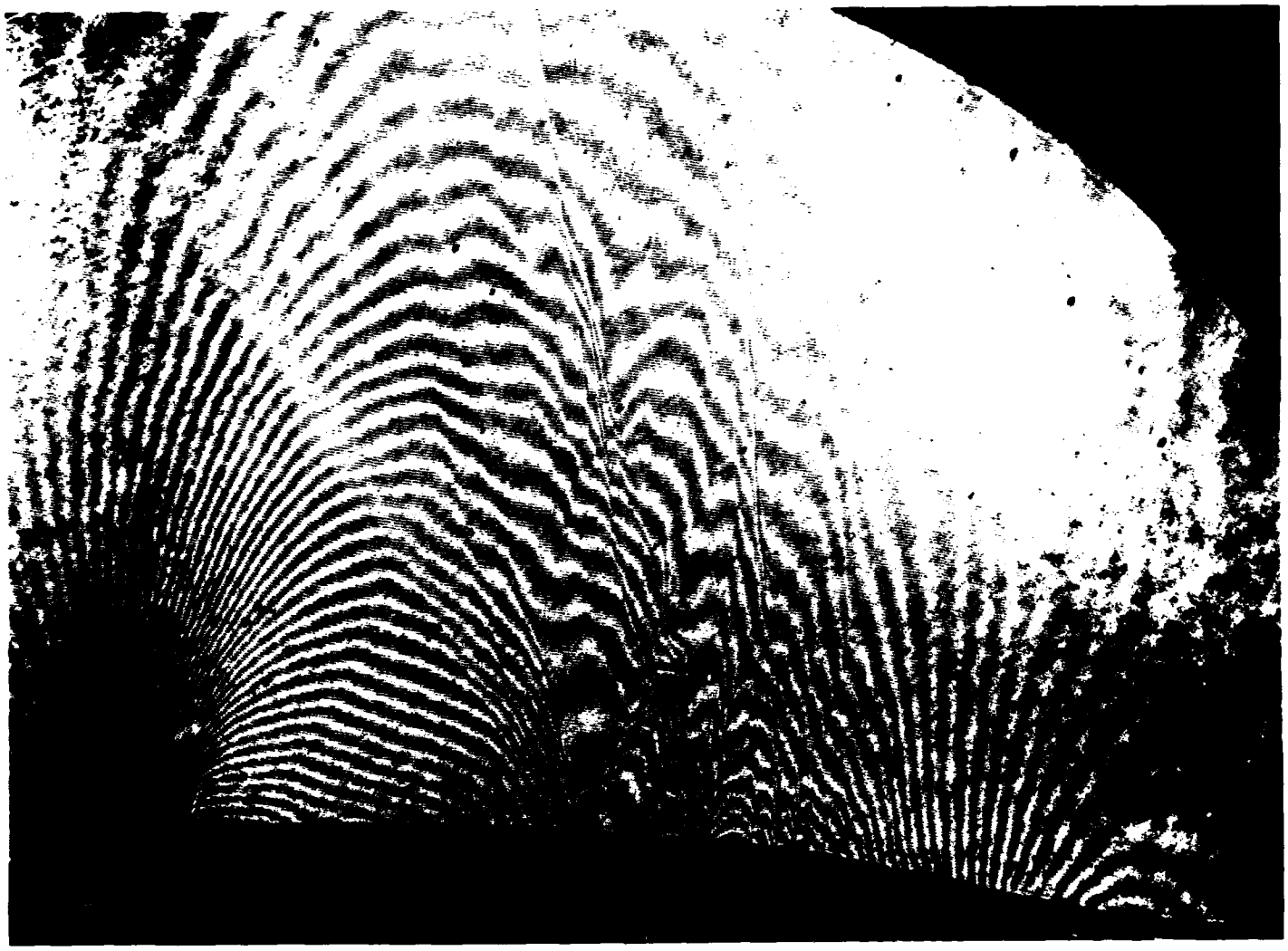

FIG. 4 PHOTOGRAPH OF INTERFEROGRAM
M = 0.783, α = 1.7°, TRANSITION FREE

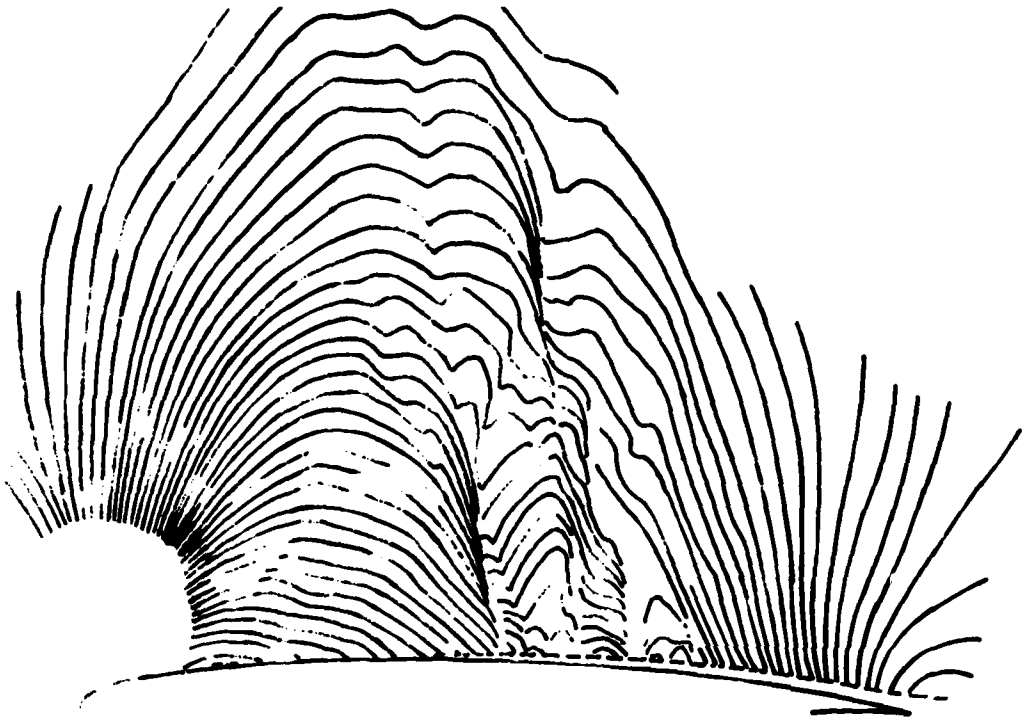

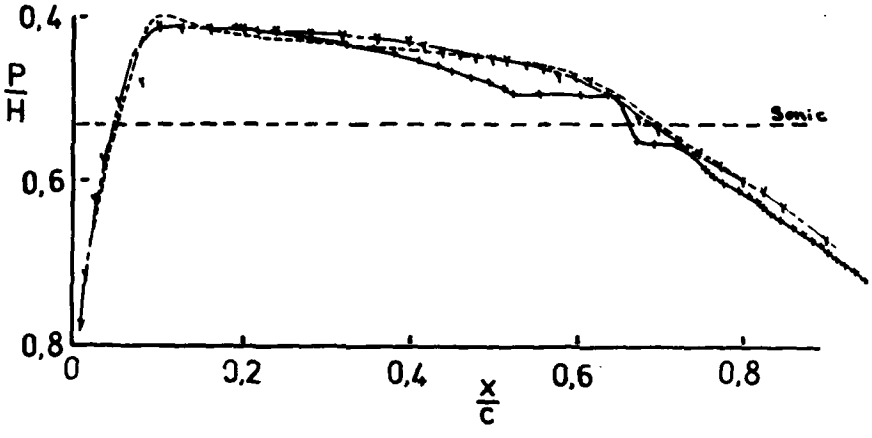

Design

From surface tappings

From interferogram

FIG. 5 INTERFEROGRAM AND PRESSURE DISTRIBUTIONS
M = 0.783, α = 1.7°, TRANSITION FREE

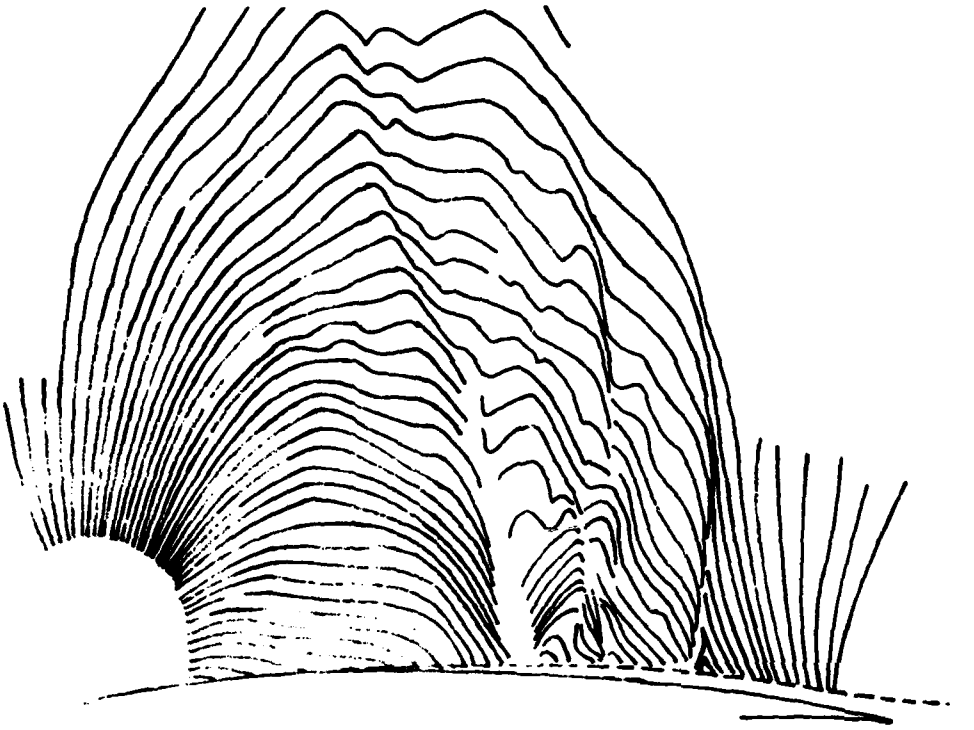

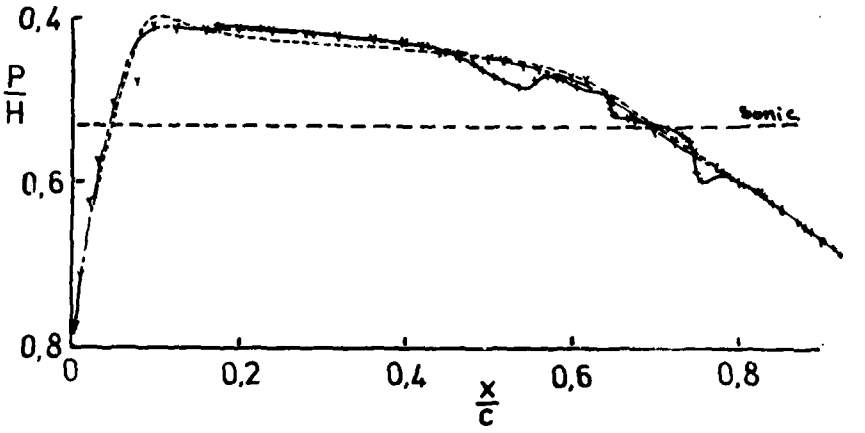

Design

From surface tappings

From interferogram

FIG. 6 INTERFEROGRAM AND PRESSURE DISTRIBUTIONS
M = 0.783, α = 1.7°, TRANSITION FREE

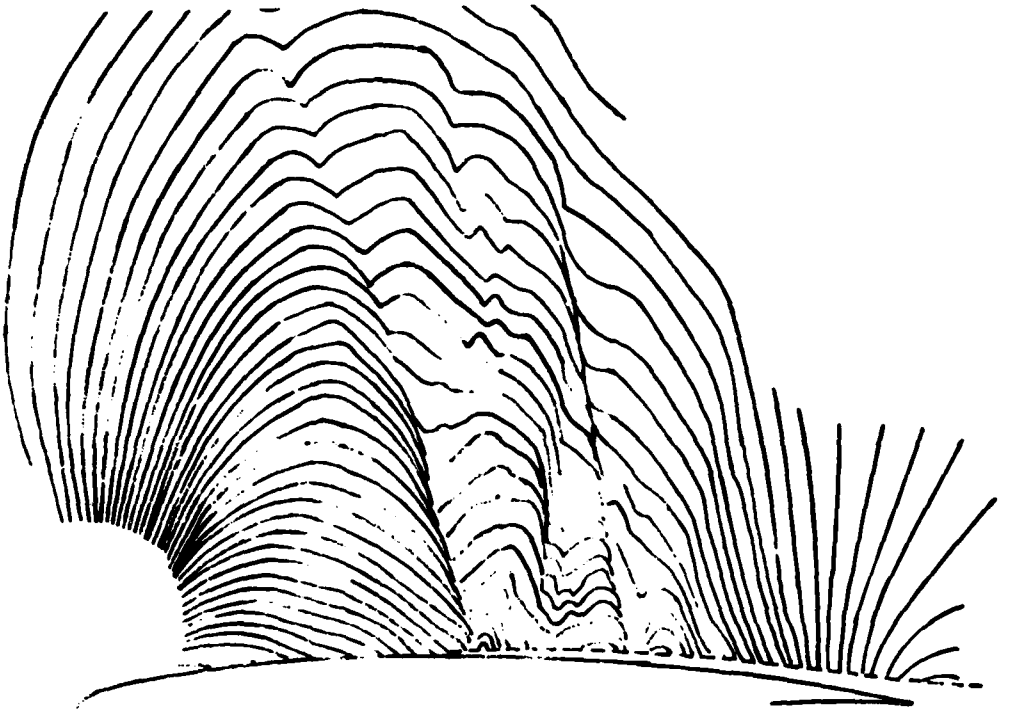

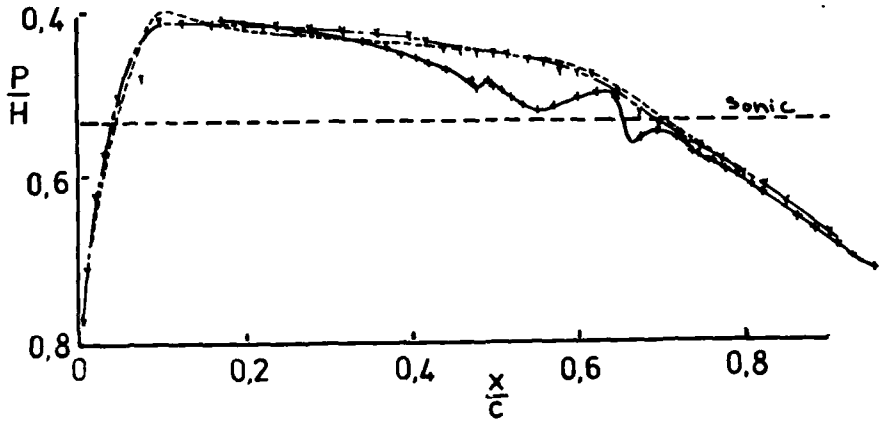

FIG. 7 INTERFEROGRAM AND PRESSURE DISTRIBUTIONS
M = 0.783, α = 1.7°, TRANSITION FREE

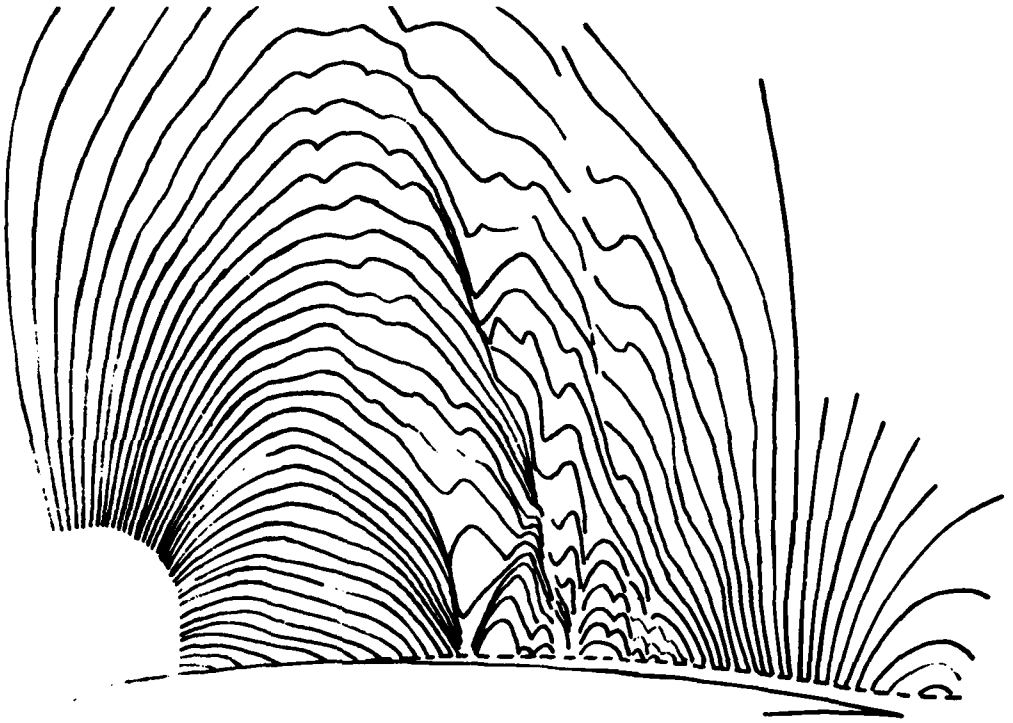

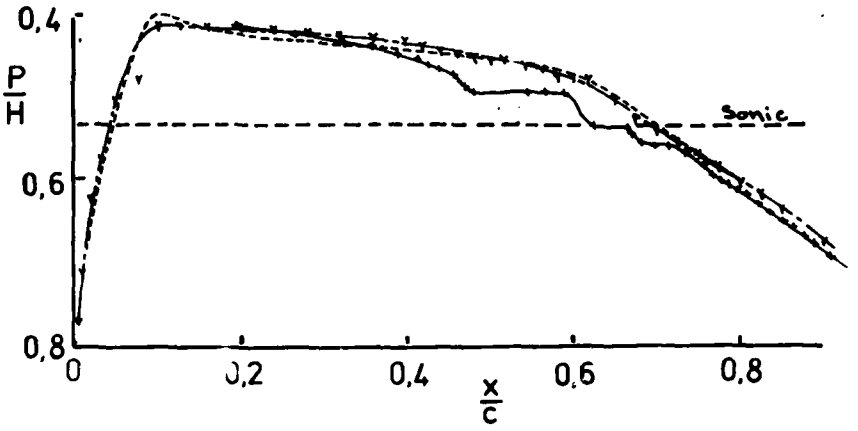

---------- Design

—v— From surface tappings

—+— From interferogram

FIG. 8 INTERFEROGRAM AND PRESSURE DISTRIBUTIONS
M = 0.783, α = 1.7°, TRANSITION FREE

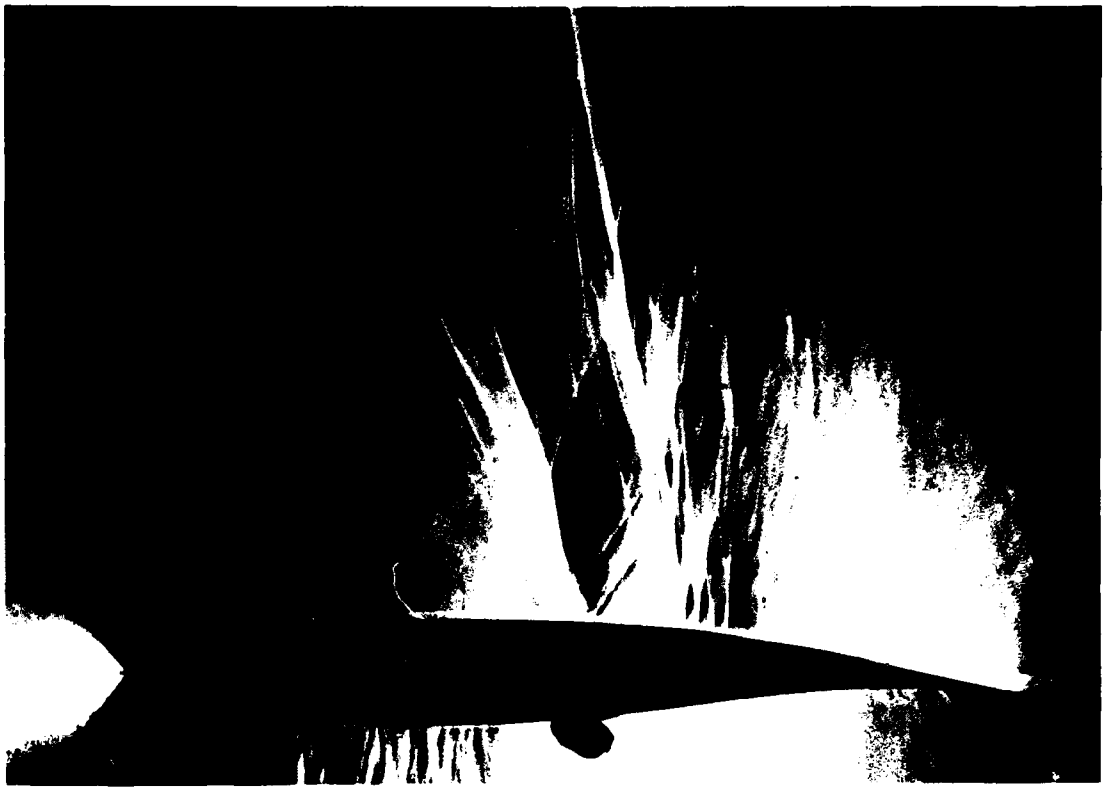

Exposure time = 1 μ sec

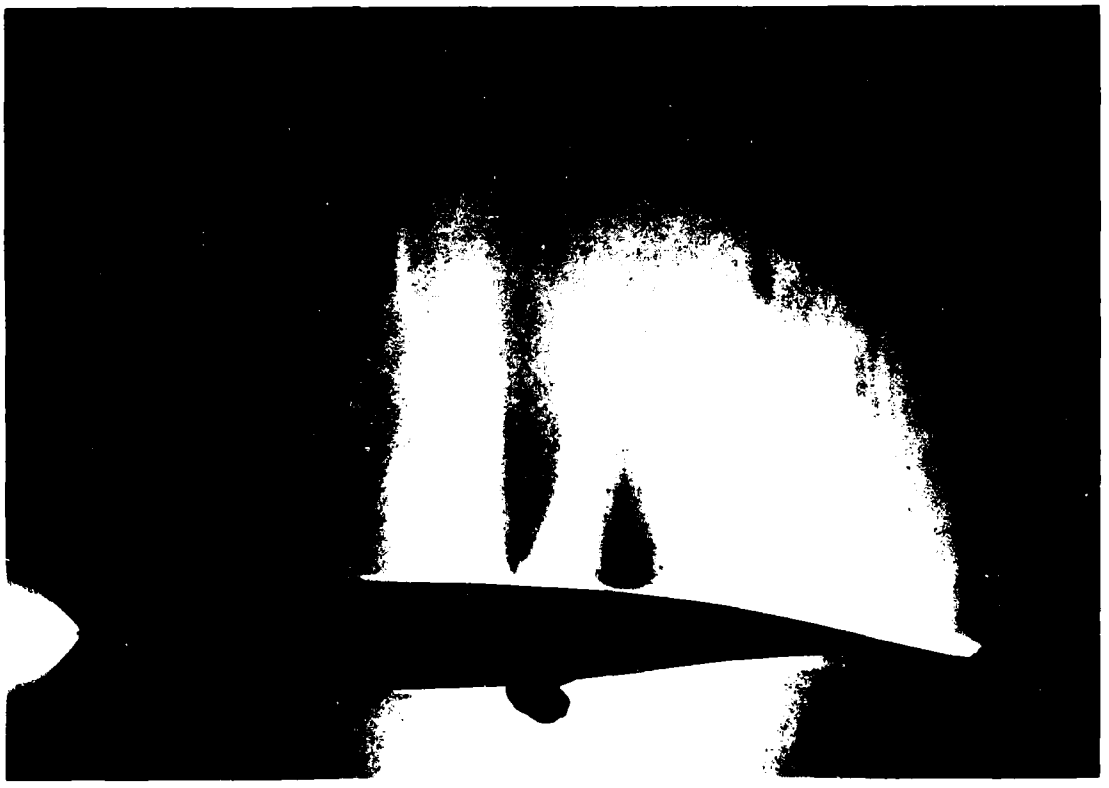

Exposure time = 20 m sec

FIG. 9 SCHLIEREN PHOTOGRAPHS
M = 0.783, α = 1.7°, TRANSITION FREE

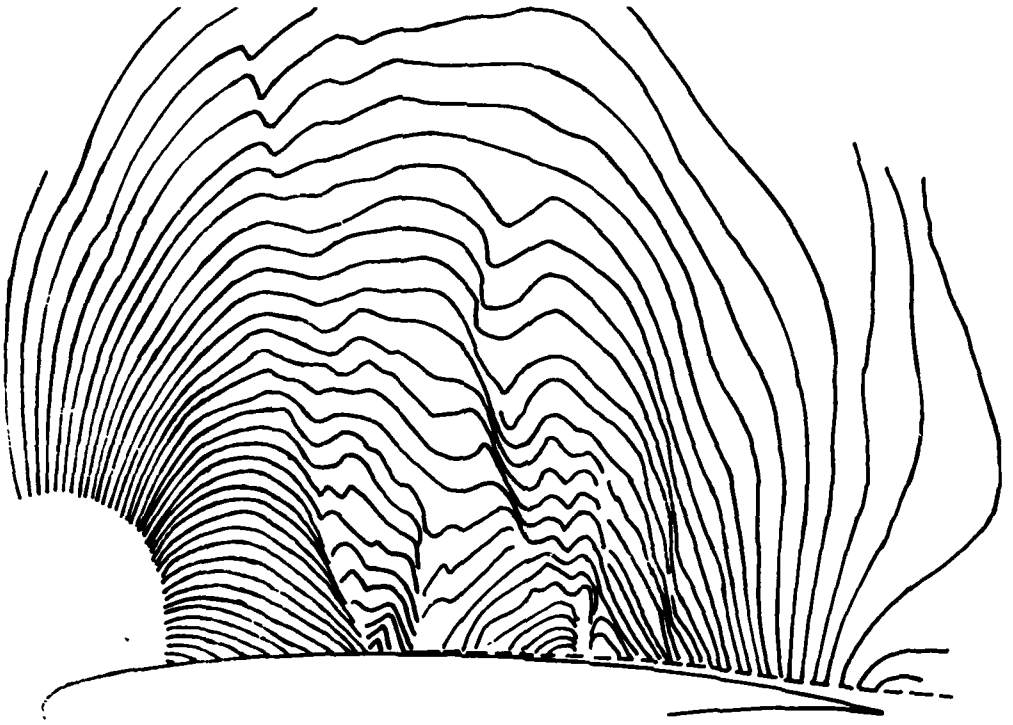

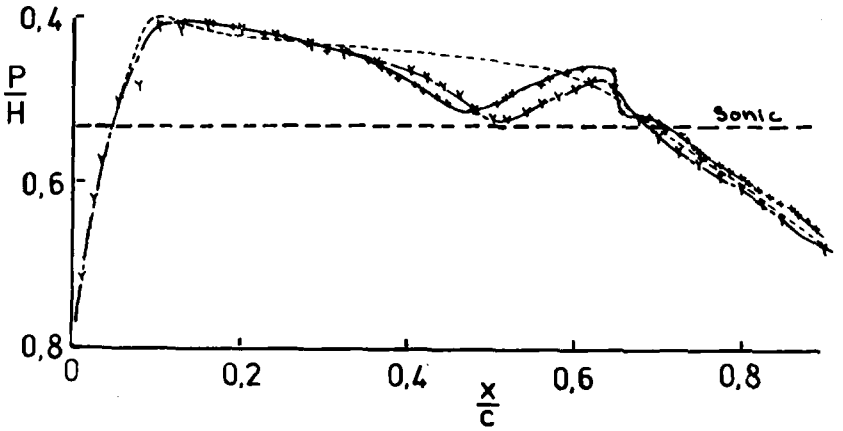

Design

From surface tappings

From interferogram

FIG. 10 INTERFEROGRAM AND PRESSURE DISTRIBUTIONS
M = 0.775, α = 1.7°, TRANSITION FREE

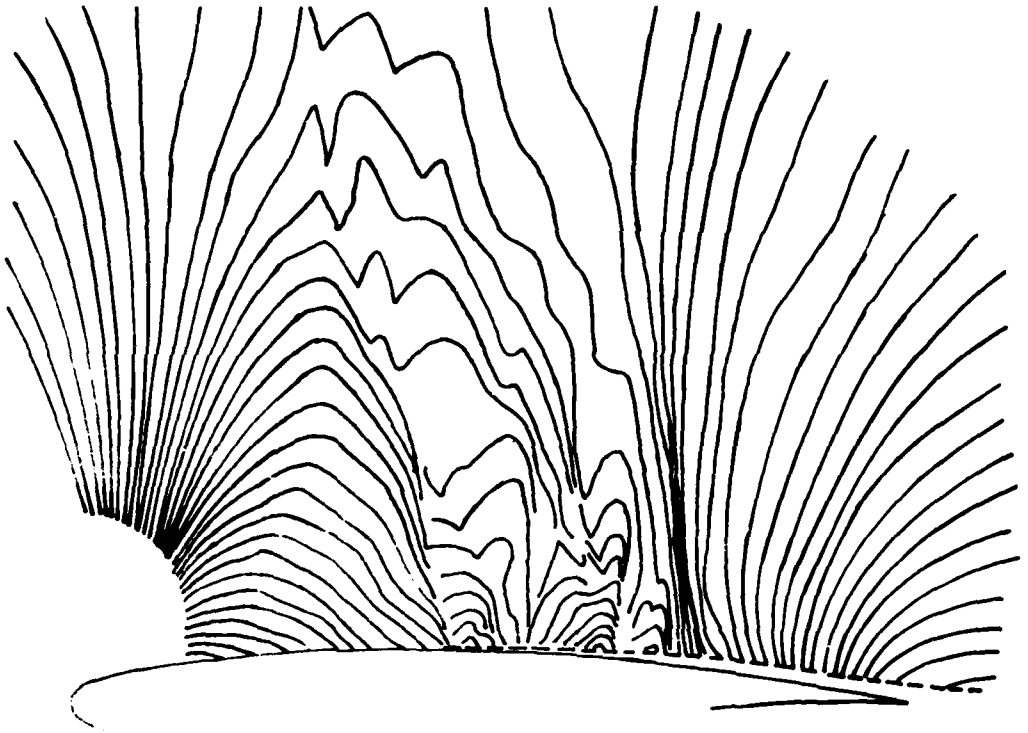

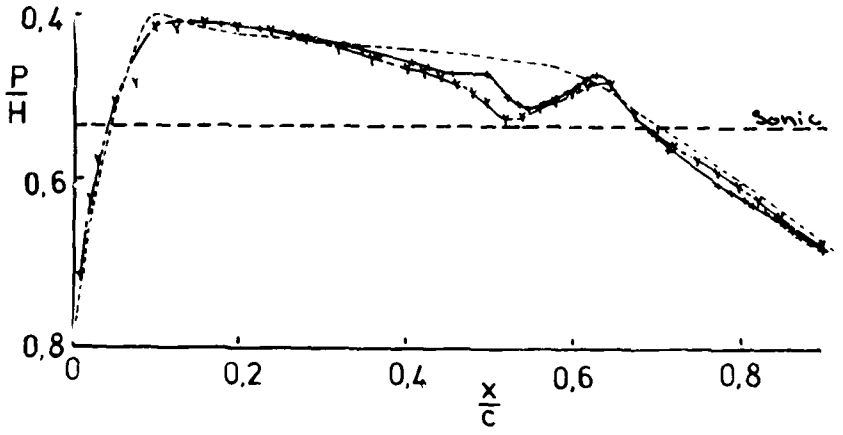

Design

From surface tappings

From interferogram

FIG. 11 INTERFEROGRAM AND PRESSURE DISTRIBUTIONS
M = 0.780, α = 1.7°, TRANSITION FREE

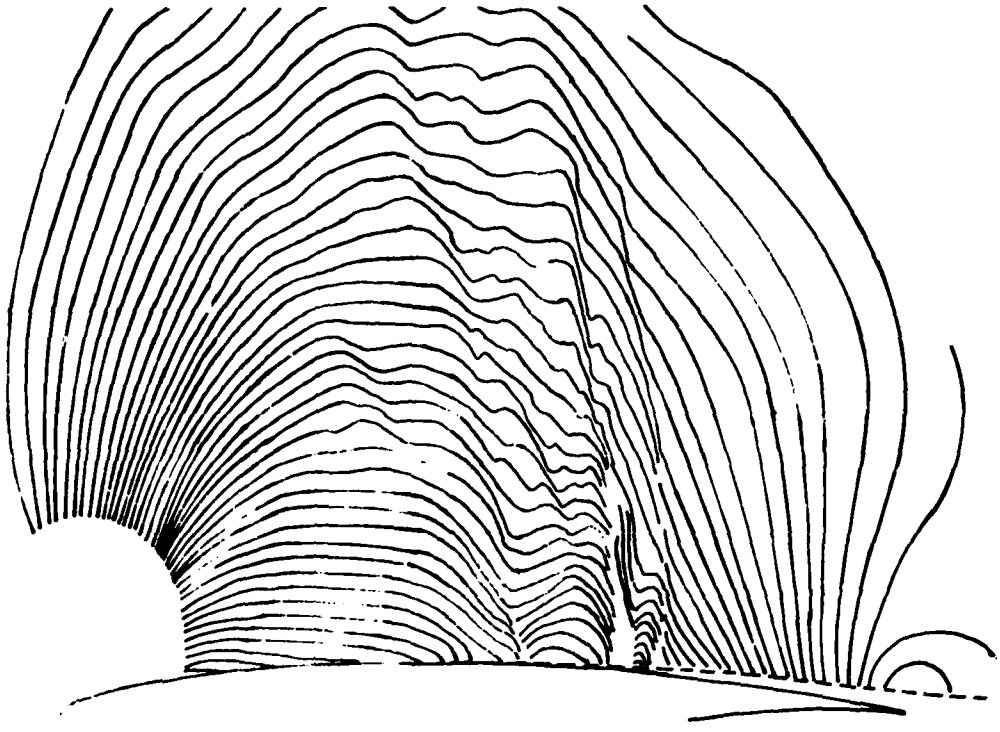

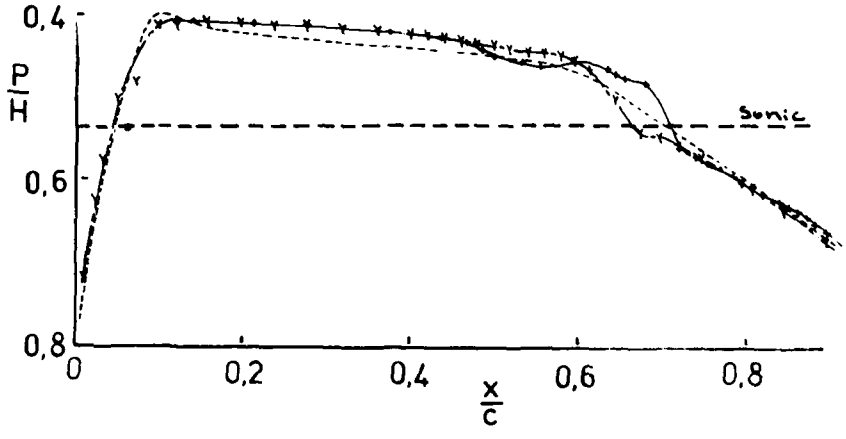

Design

From surface tappings

From interferogram

FIG. 12 INTERFEROGRAM AND PRESSURE DISTRIBUTIONS
M = 0.788, α = 1.7°, TRANSITION FREE

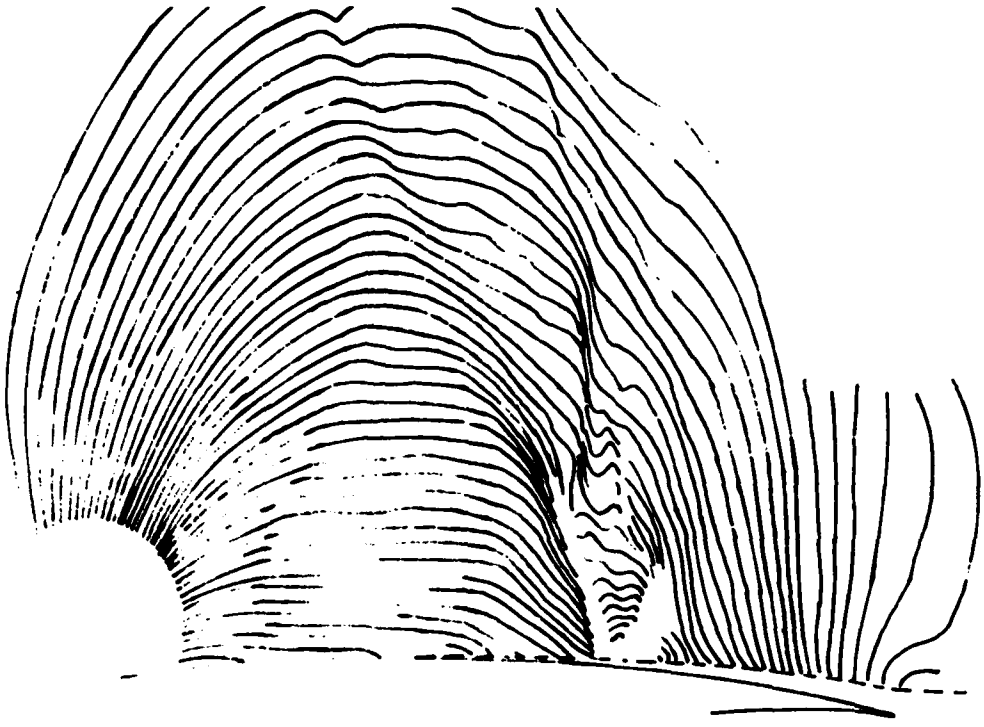

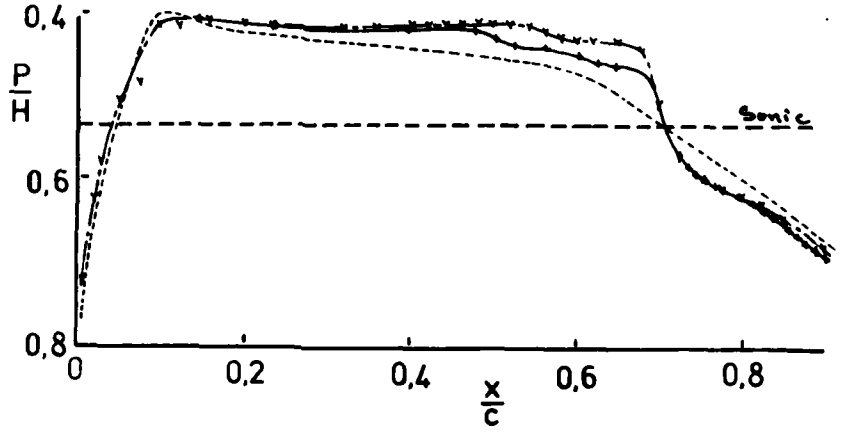

Design

From surface tappings

From interferogram

FIG. 13 INTERFEROGRAM AND PRESSURE DISTRIBUTIONS
M = 0.793, α = 1.7°, TRANSITION FREE

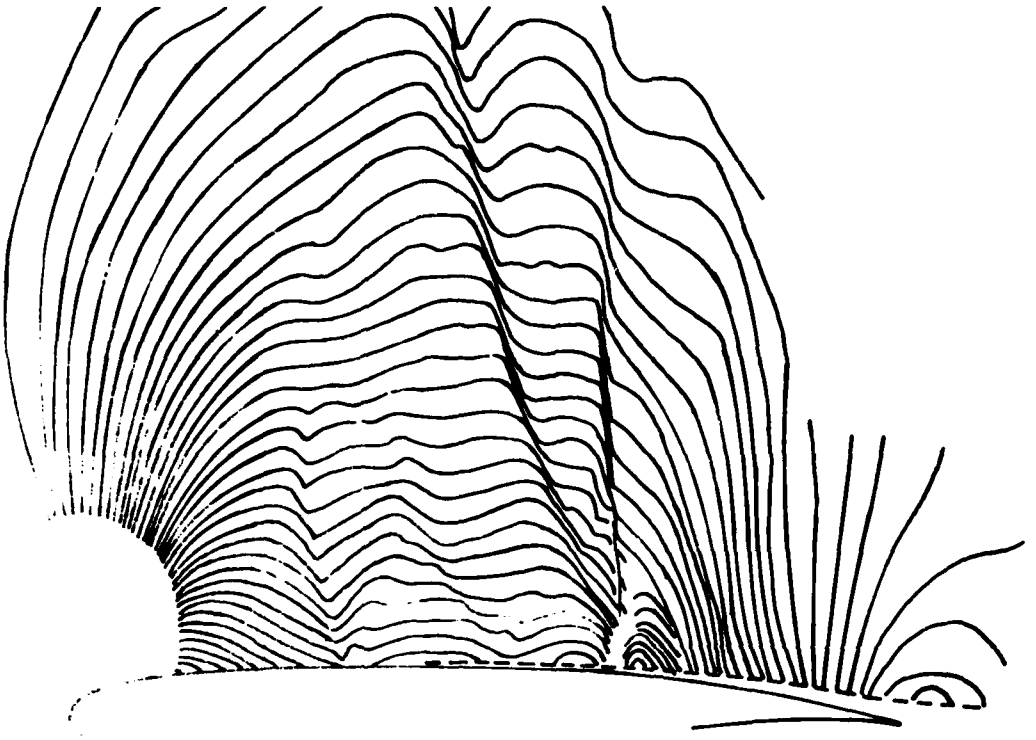

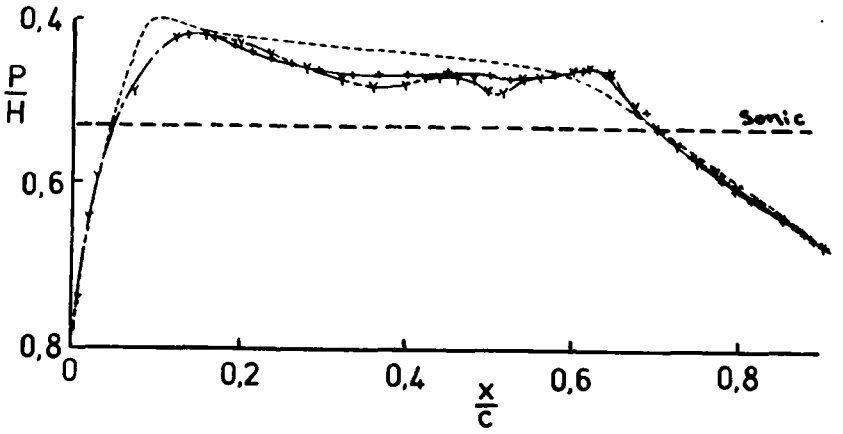

---------- Design

From surface tappings

From interferogram

FIG. 14 INTERFEROGRAM AND PRESSURE DISTRIBUTIONS
M = 0.783, α = 1.2°, TRANSITION FREE

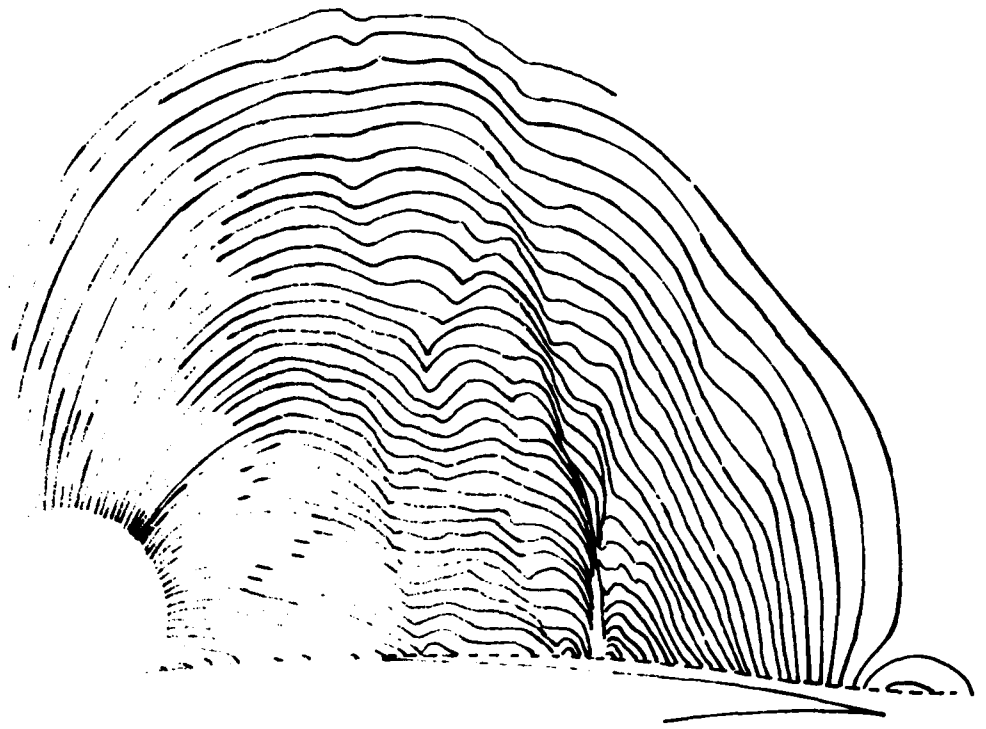

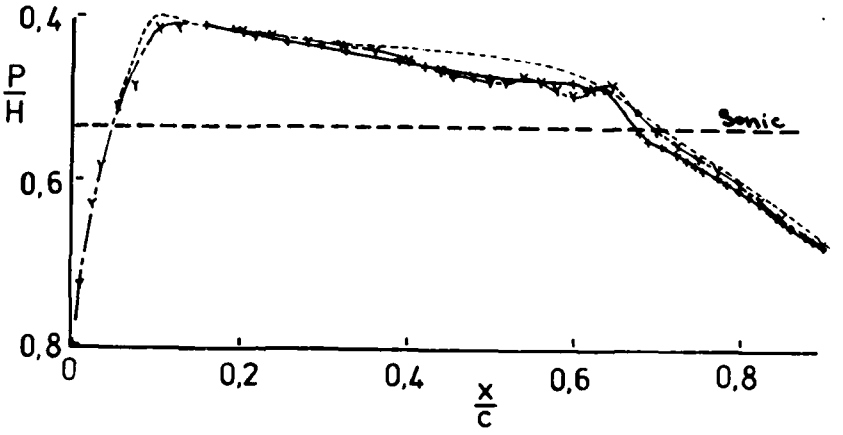

Design

From surface tappings

From interferogram

FIG. 15 INTERFEROGRAM AND PRESSURE DISTRIBUTIONS
M = 0.783, α = 1.5°, TRANSITION FREE

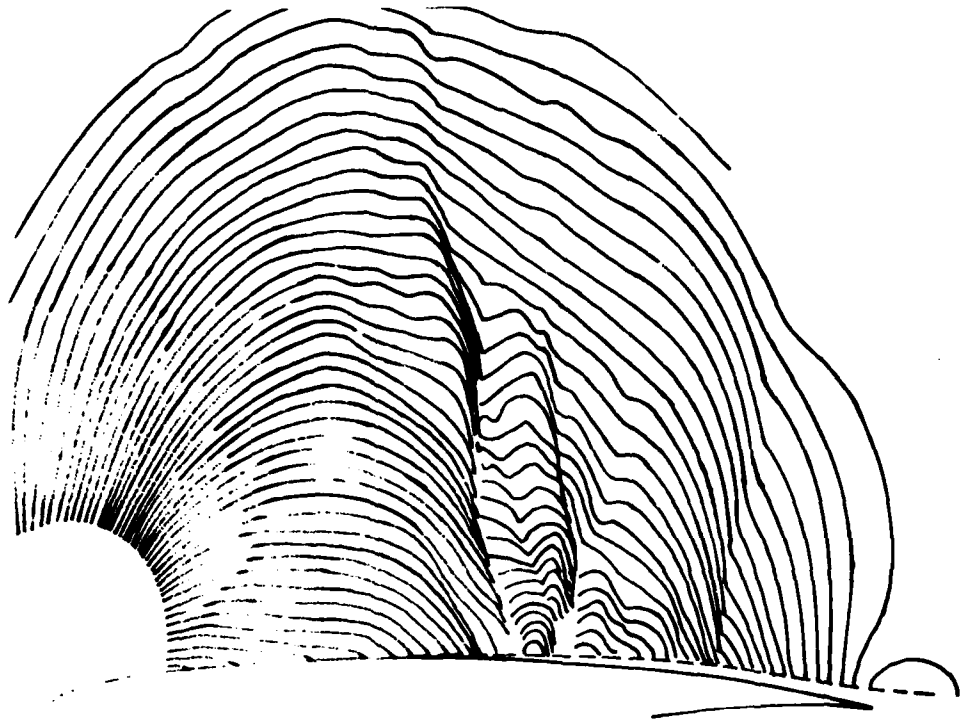

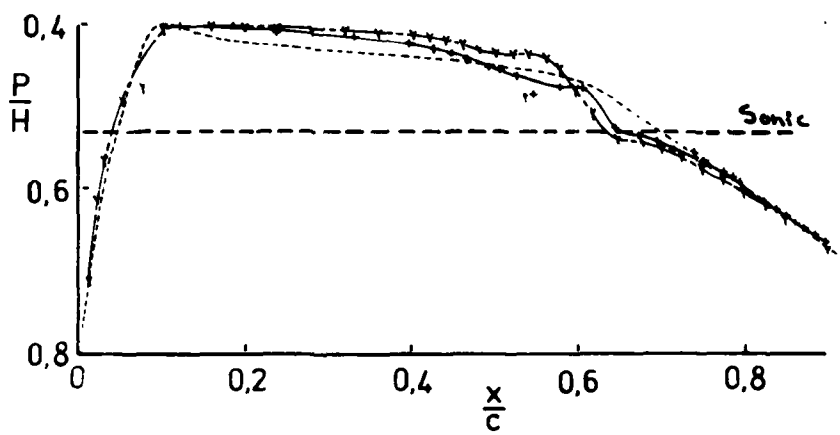

Design

From surface tappings

From interferogram

FIG. 16 INTERFEROGRAM AND PRESSURE DISTRIBUTIONS
M = 0.783, $\alpha = 1.9^{\circ}$, TRANSITION FREE

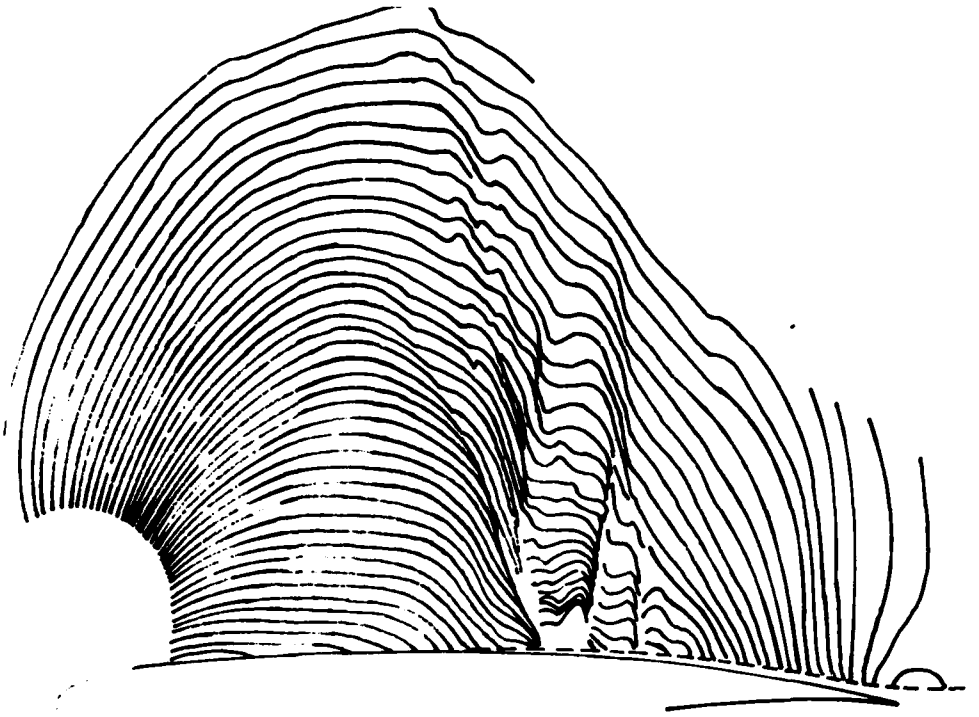

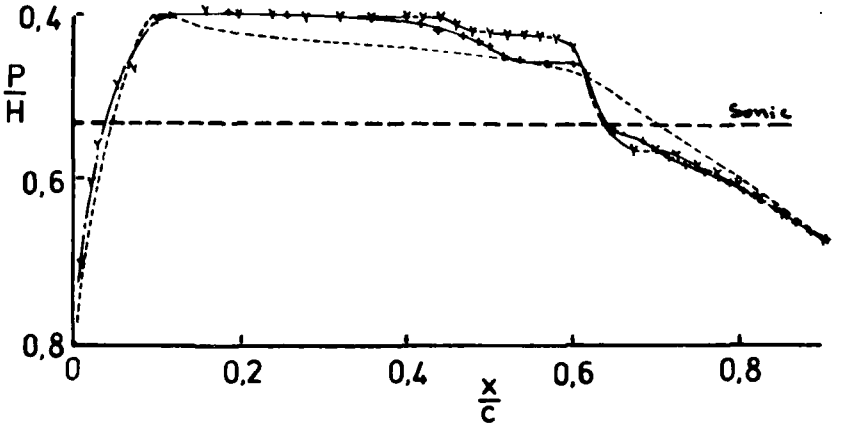

---------- Design

From surface tappings

From interferogram

FIG. 17 INTERFEROGRAM AND PRESSURE DISTRIBUTIONS
M = 0.783, $\alpha = 2.1^{\circ}$, TRANSITION FREE

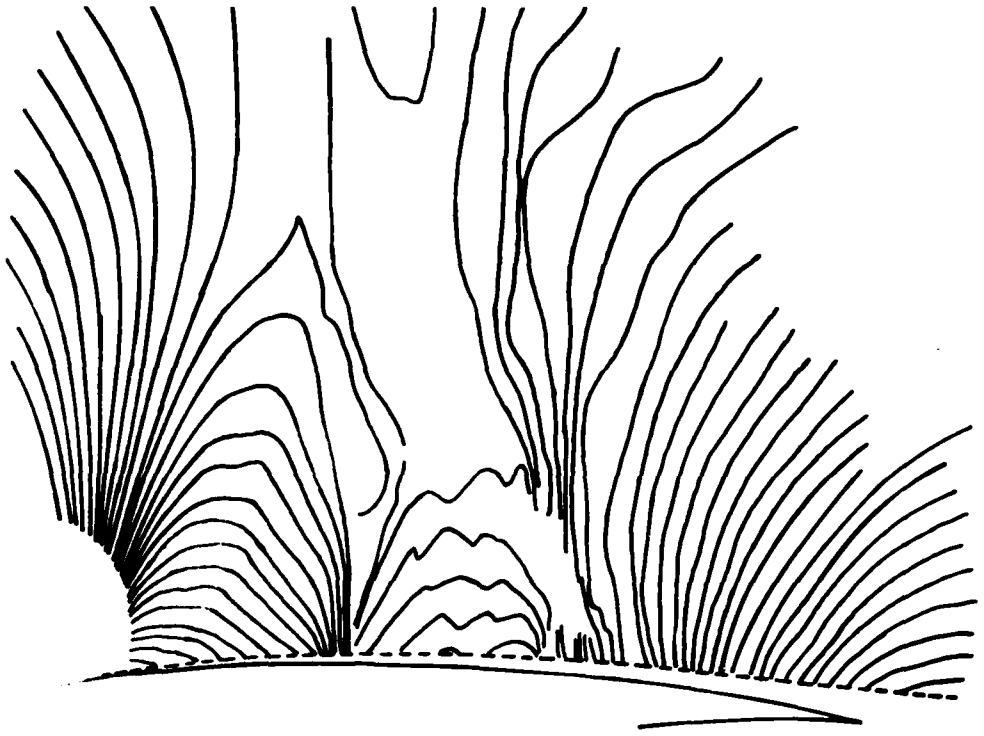

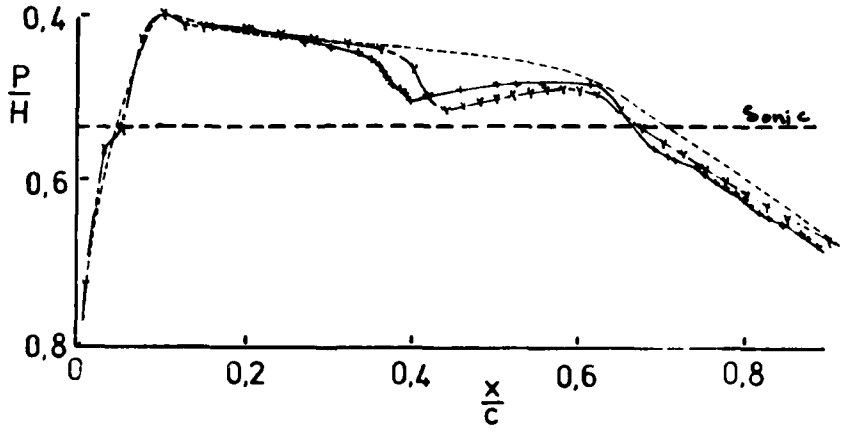

Design

From surface tappings

From interferogram

FIG. 18 INTERFEROGRAM AND PRESSURE DISTRIBUTIONS
M = 0.783, α = 1.7°, TRANSITION AT 2%C

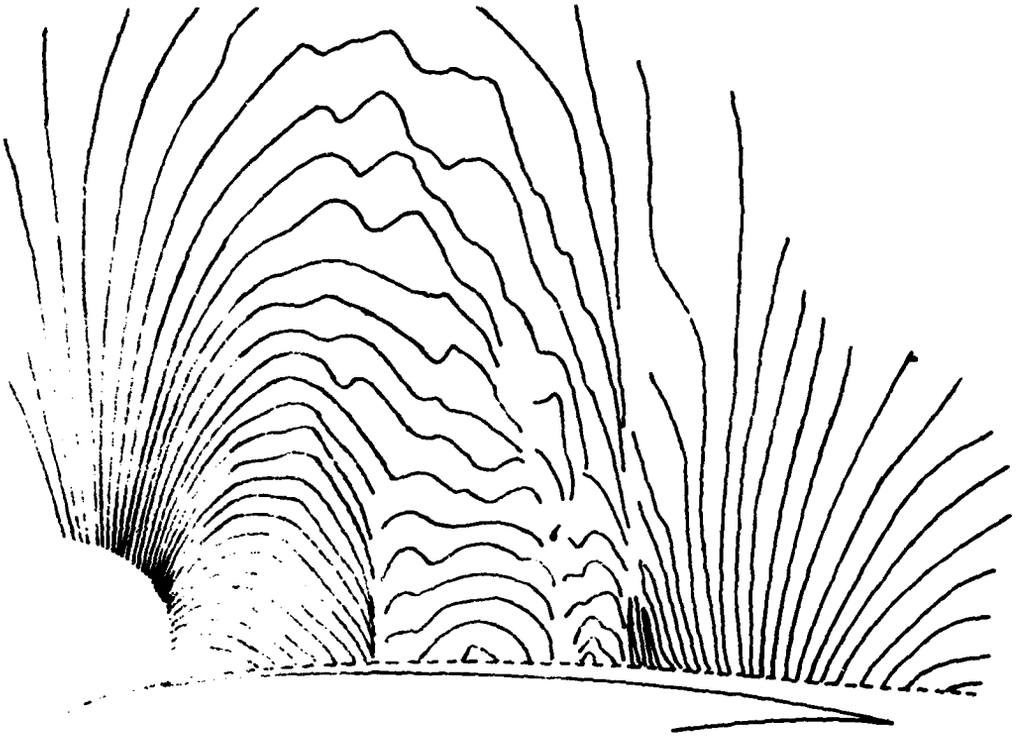

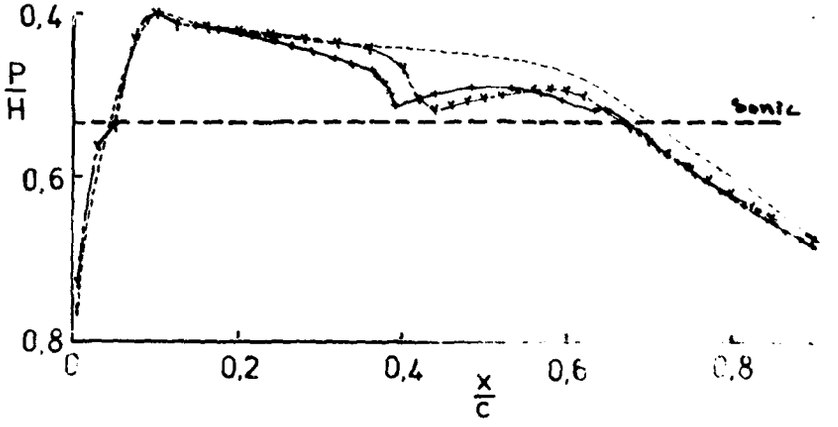

Design

From surface tappings

From interferogram

FIG. 19 INTERFEROGRAM AND PRESSURE DISTRIBUTIONS
M = 0.783, α = 1.7°, TRANSITION AT 2%C

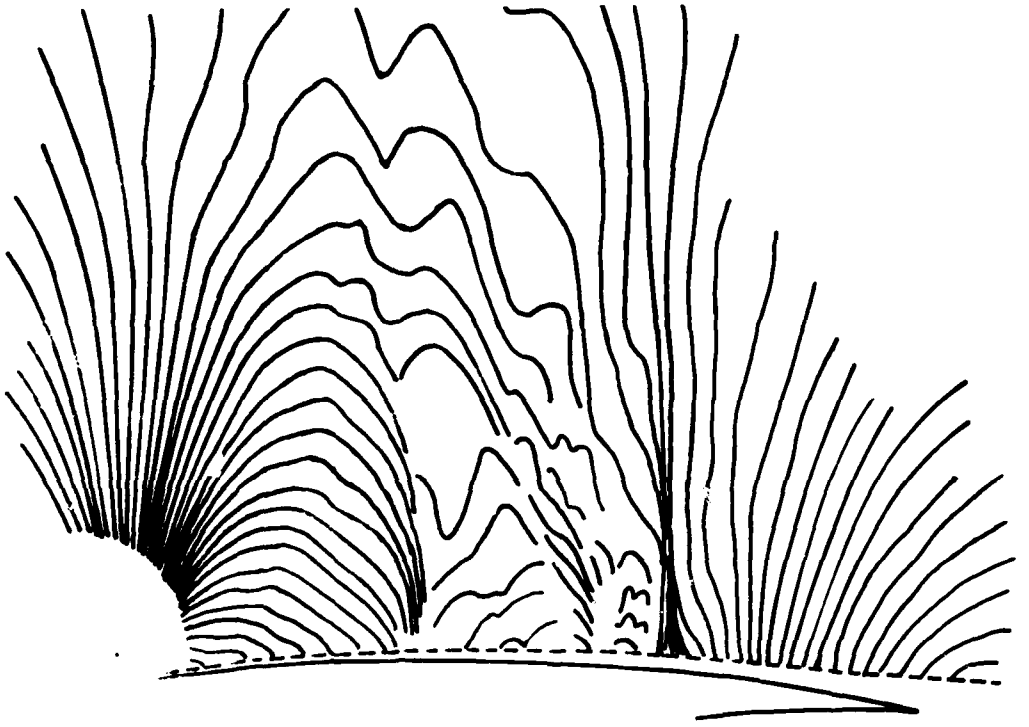

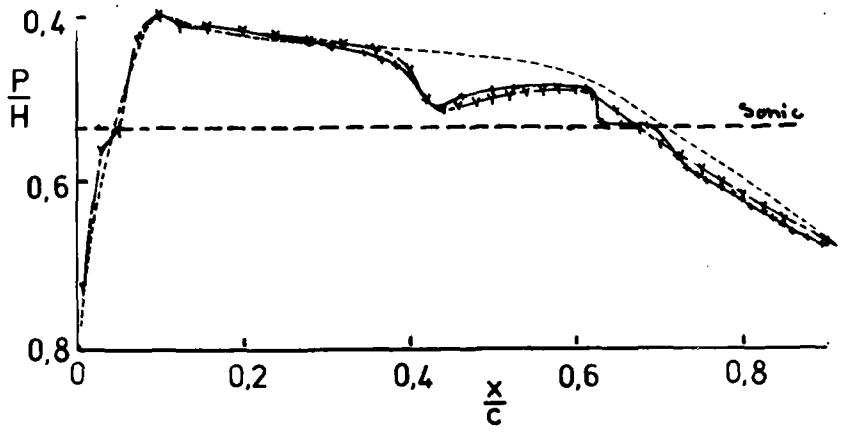

---------- Design

—x— From surface tappings

—+— From interferogram

FIG. 20 INTERFEROGRAM AND PRESSURE DISTRIBUTIONS
M = 0.783, α = 1.7°, TRANSITION AT 2%C

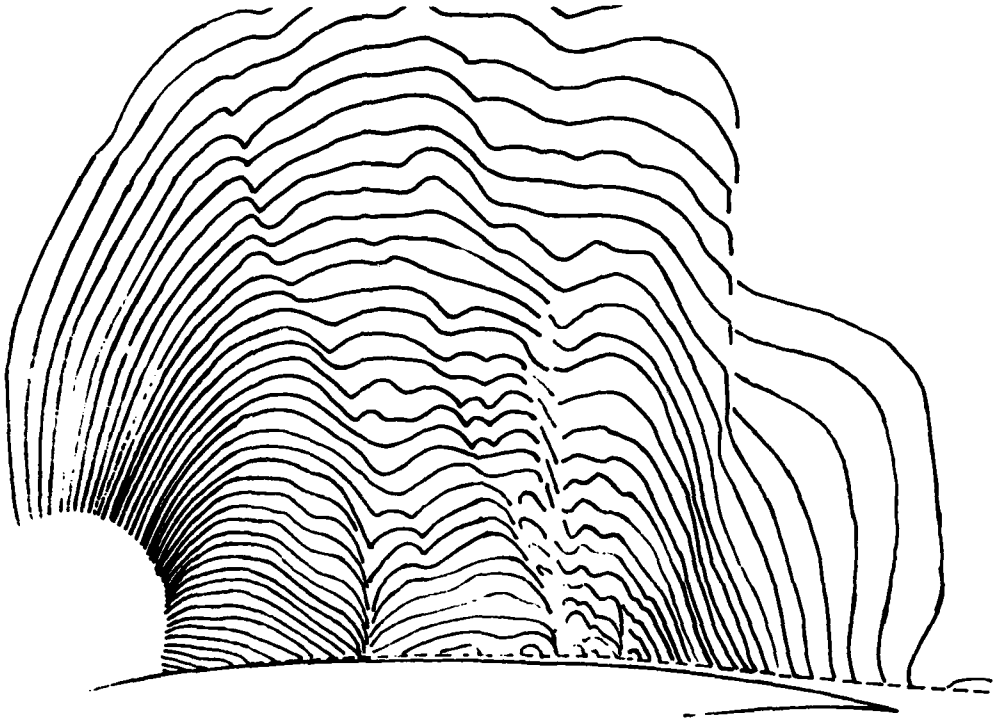

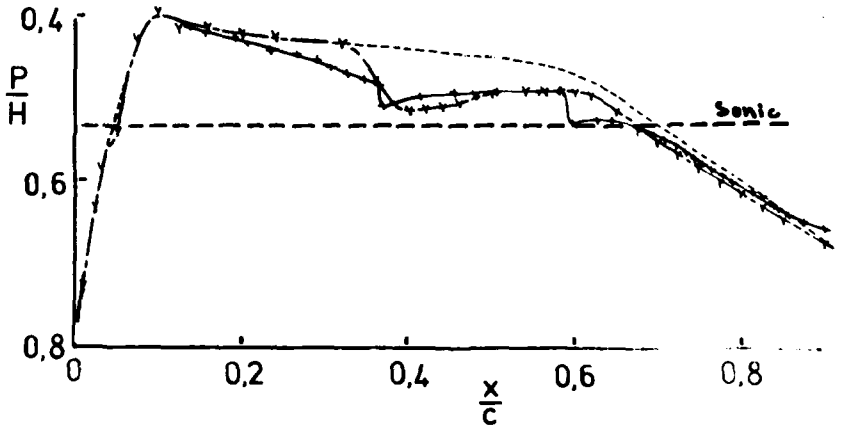

Design

From surface tappings

From interferogram

FIG. 21 INTERFEROGRAM AND PRESSURE DISTRIBUTIONS
M = 0.783, α = 1.7°, TRANSITION AT 5%C

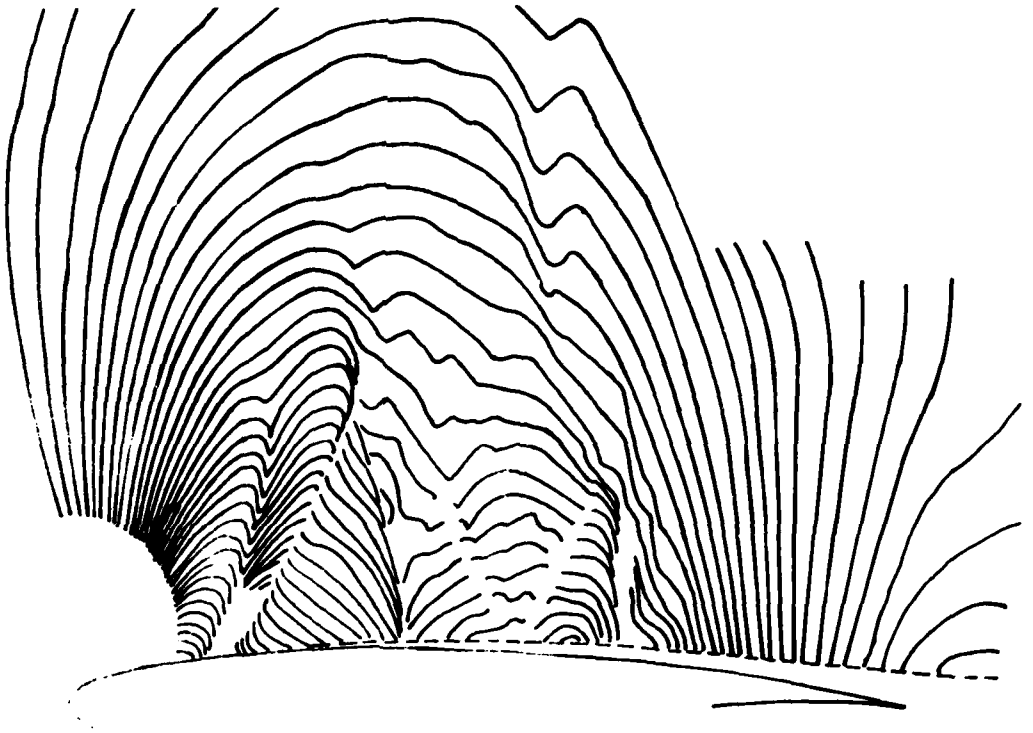

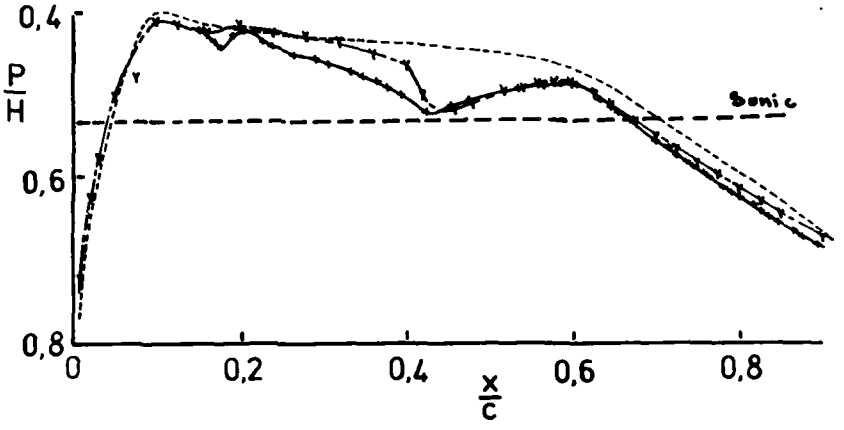

Design

From surface tappings

From interferogram

FIG. 22 INTERFEROGRAM AND PRESSURE DISTRIBUTIONS
M = 0.783, α = 1.7°, TRANSITION AT 17%C

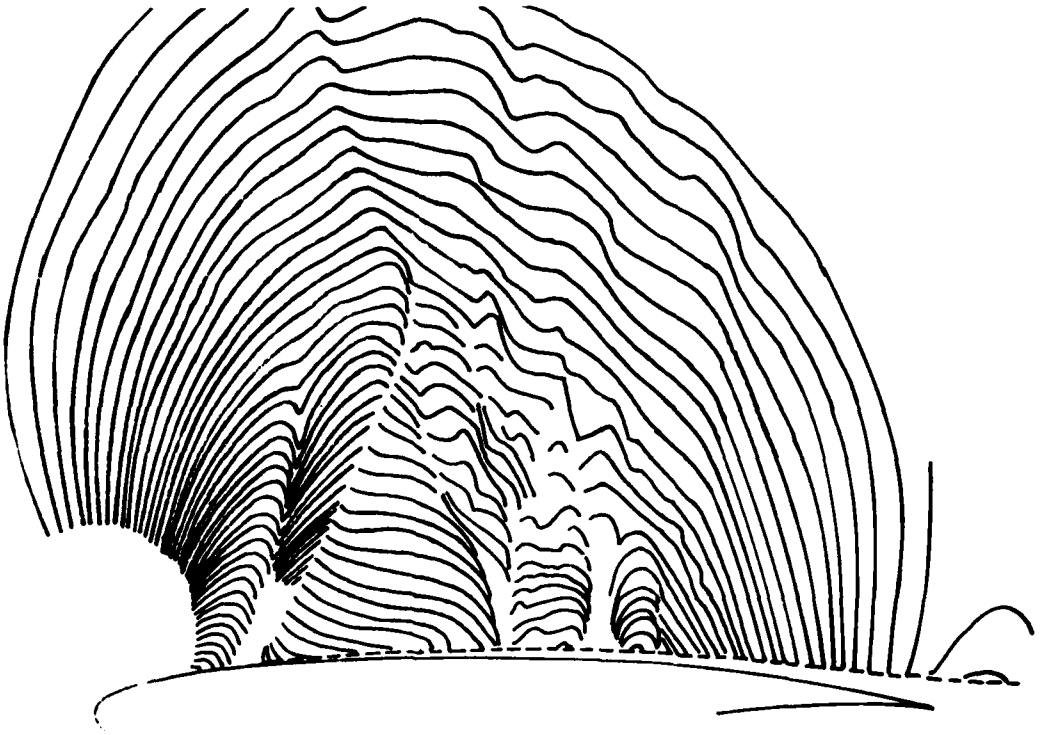

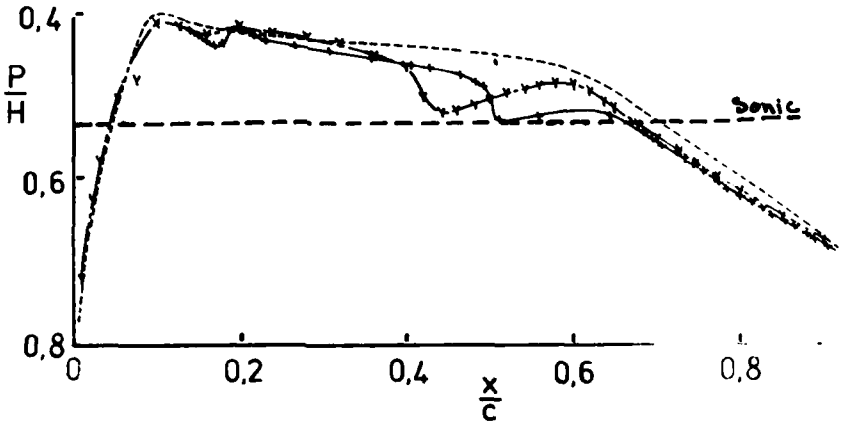

Design

From surface tappings

From interferogram

FIG. 23 INTERFEROGRAM AND PRESSURE DISTRIBUTIONS
M = 0.783, α = 1.7°, TRANSITION AT 17%C

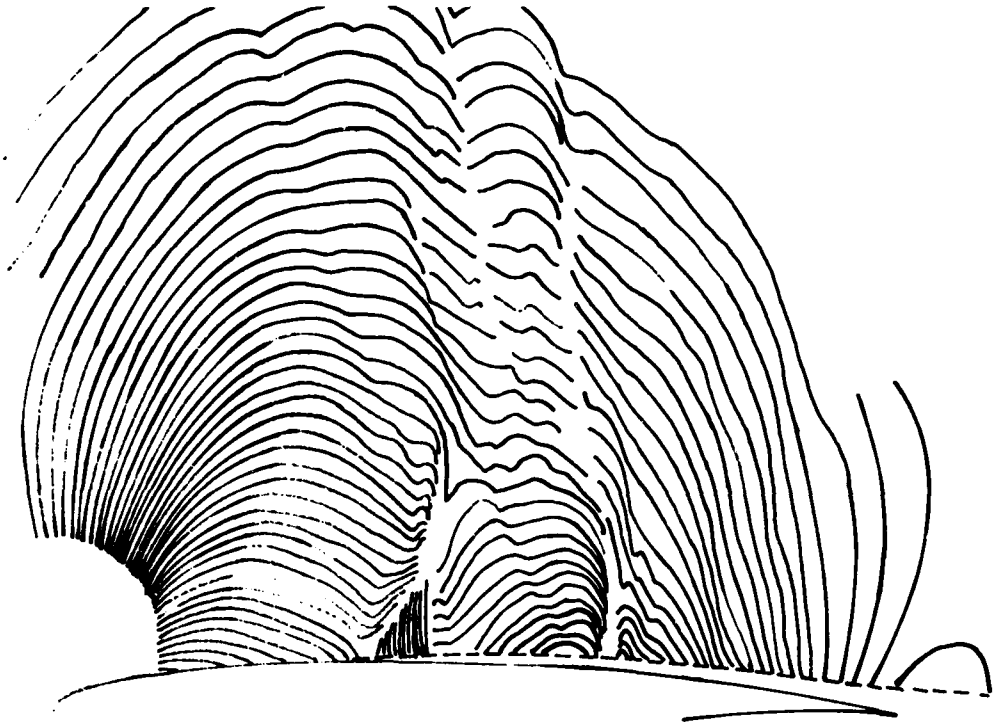

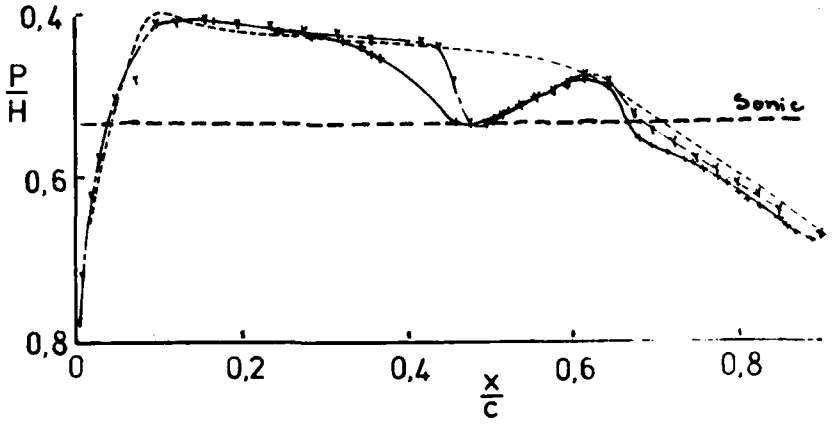

Design

From surface tappings

From interferogram

FIG. 24 INTERFEROGRAM AND PRESSURE DISTRIBUTIONS
M = 0.783, α = 1.7°, TRANSITION AT 37%C

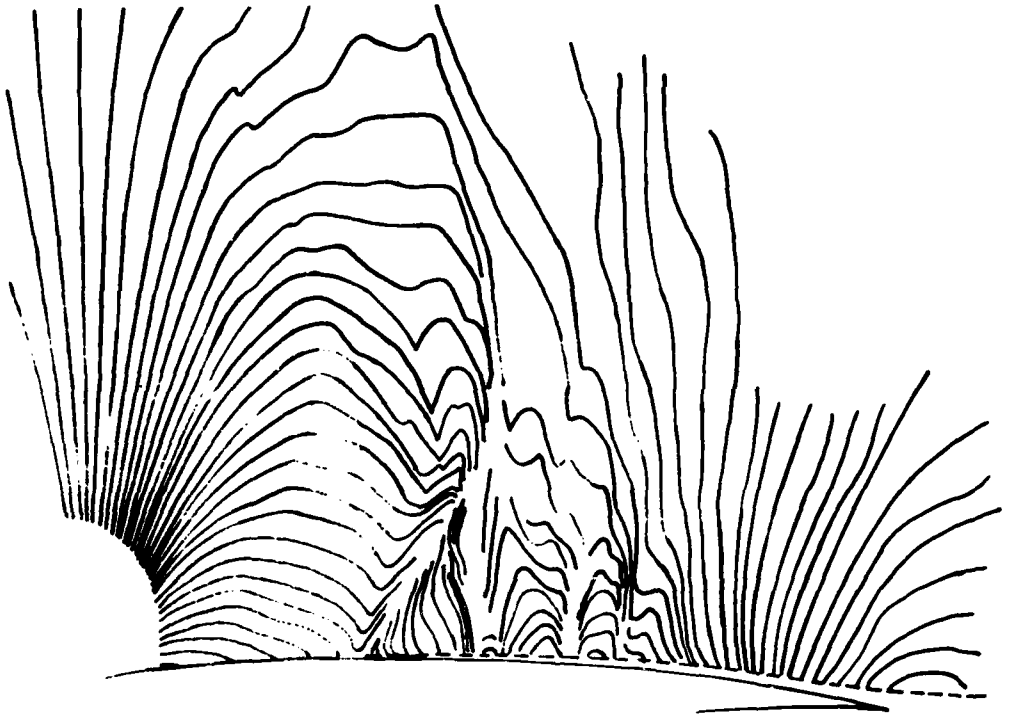

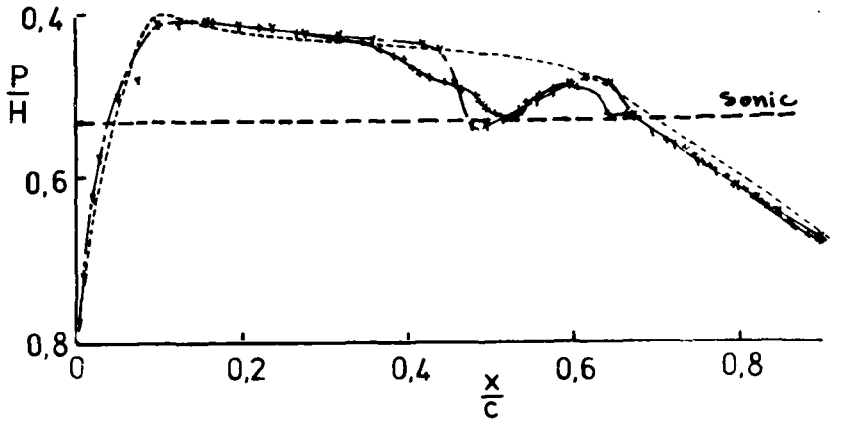

Design

From surface tappings

From interferogram

FIG. 25 INTERFEROGRAM AND PRESSURE DISTRIBUTIONS
M = 0.783, α = 1.7°, TRANSITION AT 37%C

DISTRIBUTION

Copy No.

AUSTRALIA

Department of Defence

Central Office

Chief Defence Scientist	1
Deputy Chief Defence Scientist	1
Superintendent, Science and Technology Programmes	1
Controller, Programmes and Analytical Studies	1
Aust. Defence Scientific and Technical Rep. (U.K.)	—
Counsellor, Defence Science (U.S.A.)	—
Defence Central Library	2
Document Exchange Centre, D.I.S.B. (17)	3–19
Joint Intelligence Organisation	20

Aeronautical Research Laboratories

Chief Superintendent	21
Library	22
Superintendent Aerodynamics	23
Divisional File-Aerodynamics	24
Transonic Wind Tunnel Group	25–28
Author: N. Pollock	29

Materials Research Laboratories

Library	30

Defence Research Centre

Library	31

Central Office

Director General—Army Development (NSO) (4)	32–35

Engineering Development Establishment

Library	36

Navy Office

Naval Scientific Adviser	37

Army Office

Army Scientific Adviser	38
Royal Military College Library	39
US Army Research, Development and Standardisation Group	40

Air Force Office

Aircraft Research and Development Unit, Scientific Flight Group	41
Library	42
Air Force Scientific Adviser	43
Technical Division Library	44
HQ Support Command [SENGSO]	45
RAAF Academy, Point Cook	46

Department of Industry and Commerce

Government Aircraft Factories

Manager		47
Library		48

Statutory and State Authorities and Industry

Australian Atomic Energy Commission, Director		49
SEC of Vic., Herman Research Laboratory, Library		50
Ansett Airlines of Australia, Library		51
B.H.P., Melbourne Research Laboratories		52

Universities and Colleges

Adelaide	Barr Smith Library	53
	Professor of Mechanical Engineering	54
Latrobe	Library	55
Melbourne	Engineering Library	56
Monash	Hargrave Library	57
Newcastle	Library	58
Sydney	Engineering Library	59
N.S.W.	Physical Sciences Library	60
Queensland	Library	61
Western Australia	Library	62
	Associate Professor J. A. Cole, Mechanical Engineering	63
R.M.I.T.	Library	64

CANADA

NRC

Aeronautical and Mechanical Engineering Library	65
Gas Dynamics Laboratory, Mr R. A. Tyler	66

FRANCE

ONERA, Library	67

INDIA

Defence Ministry, Aero Development Establishment, Library	68
Hindustant Aeronautics Ltd, Library	69
National Aeronautical Laboratory, Information Centre	70

ISRAEL

Technion-Israel Institute of Technology, Professor J. Singer	71

NETHERLANDS

National Aerospace Laboratory [NLR], Library	72

NEW ZEALAND

Universities

Canterbury	Library	73
	Professor D. Stevenson, Mechanical Eng.	74

SWEDEN

Aeronautical Research Institute, Library	75

SWITZERLAND

F+W (Swiss Federal Aircraft Factory)	76

DOCUMENT CONTROL DATA

1. a. AR No	1. b. Establishment No	2. Document Date	3. Task No
AR-002-328	ARL-Aero-Note-405	January, 1982	DST 79/107

4. Title	5. Security	6. No Pages
AN INTERFEROMETRIC INVESTIGATION OF THE NEAR DESIGN POINT FLOW OVER SUPERCRITICAL AEROFOIL BGK-1	a. document Unclassified b. title u c. abstract u	12 7. No Refs 14

8. Author(s)	9. Downgrading Instructions
N. Pollock	—

10. Corporate Author and Address	11. Authority (*as appropriate*)
Aeronautical Research Laboratories G.P.O. Box 4331, Melbourne, Vic. 3001	a. Sponsor b. Security c. Downgrading d. Approval

12. Secondary Distribution (*of this document*)
Approved for public release

Overseas enquirers outside stated limitations should be referred through ASDIS, Defence Information Services Branch, Department of Defence, Campbell Park, CANBERRA ACT 2601

13. a. This document may be ANNOUNCED in catalogues and awareness services available to . . .

No limitations

13. b. Citation for other purposes (*i.e. casual announcement*) may be unrestricted

14. Descriptors		15. COSATI Group
Interferometers	Airfoils	2004
Two dimensional flow	Transonic air foils	0101
Transonic flow	Wind tunnel tests	

16.

ABSTRACT

A recently developed laser interferometer was used to study the upper surface flow over supercritical aerofoil BGK-1 near its design condition. The tests were carried out at a chord Reynolds number of $1{\cdot}65 \times 10^6$ with transition free and artificially fixed at various chordwise locations. The interferograms were analysed to produce "instantaneous" surface pressure distributions for comparison with conventional time averaged distributions obtained from surface tappings.

The results show that the upper surface flow is unsteady with both fixed and free transition. They also indicate that artificially fixing transition in low Reynolds number tests does not produce an accurate simulation of the high Reynolds number flow for conditions near the design point.

17. Imprint
Aeronautical Research Laboratories, Melbourne

18. Document Series and Number	19. Cost Code	20. Type of Report and Period Covered
Aerodynamics Note 405	54 7710	

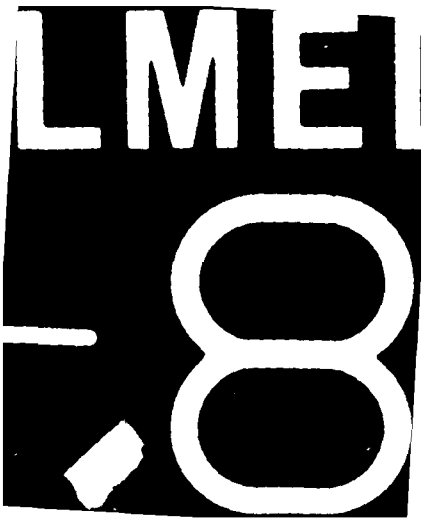
LME
.8